

STRESS-DEPENDENT FRACTURE CONDUCTIVITY OF PROPPED FRACTURES IN  
THE STIMULATED RESERVOIR VOLUME OF A HYDRAULICALLY FRACTURED  
SHALE WELL

by

Di Zhang

**Copyright by Di Zhang, 2016**

All Rights Reserved

A thesis submitted to the Faculty and the Board of Trustees of the Colorado School of Mines in partial fulfillment of the requirements for the degree of Master of Science (Petroleum Engineering).

Golden, Colorado

Date: \_\_\_\_\_

Signed: \_\_\_\_\_

Di Zhang

Signed: \_\_\_\_\_

Dr. Hazim H. Abass  
Thesis Advisor

Golden, Colorado

Date: \_\_\_\_\_

Signed: \_\_\_\_\_

Dr. Erdal Ozkan  
Professor and Head  
Department of Petroleum Engineering

## ABSTRACT

The concept of stimulated reservoir volume (SRV) has been brought to the industry to stand for the shale formation areas that have been touched by hydraulic fracturing during treatment. It is a complex fracture system that allows low permeability shale plays to be productive. Recent research on shale play development has mainly focused on achieving a better understanding of the SRV system and its potential.

This research aims to study SRV areas that are not well propped by conventional proppant and to quantify the contribution of these areas to the overall conductivity distribution. In addition, ultralight weight (ULW) proppant and clustered proppant fracturing are studied as they are two techniques that have potential to improve the production from SRV in shale plays.

Fractures propped by conventional proppants, ULW proppants and clustered proppants were analyzed through laboratory testing. The fracture permeability architecture, the permeability from natural fracture to opened fracture and to fractures with low proppant concentration, were also studied. The different properties of ULW proppant in shale rocks were studied. A numerical model that could account for various controlling factors in clustered proppant fracturing was built. These results could act as insightful reference for field applications.

## TABLE OF CONTENTS

ABSTRACT.....	iii
LIST OF FIGURES .....	vii
LIST OF TABLES .....	x
ACKNOWLEDGEMENTS.....	xi
CHAPTER 1 INTRODUCTION .....	1
1.1 Research Objectives .....	2
1.2 Research Motivations .....	3
1.3 Research Contributions .....	3
CHAPTER 2 LITERATURE REVIEW.....	5
2.1 Water Fracturing in Shale Plays .....	5
2.2 Stimulated Reservoir Volume.....	6
2.3 Stress Dependent Conductivity .....	7
2.4 Fracture Effectiveness .....	13
2.5 ULW Proppant.....	14
2.6 Partial Monolayer.....	15
2.7 Clustered Proppant Fracturing.....	17
2.8 Summary .....	18
CHAPTER 3 LABORATORY EXPERIMENT.....	20
3.1 Research Plan .....	20
3.2 Sample Preparation.....	20

3.3	Test Equipment and Method.....	23
3.4	Verification of Test Method.....	24
3.5	Critical Monolayer Concentration.....	27
CHAPTER 4 LABORATORY EXPERIMENT RESULTS.....		30
4.1	Naturally Fractured Shale Sample.....	30
4.2	Opened Fractures.....	33
4.3	Proppant Test.....	35
4.3.1	Lightweight Ceramic (LWC) 40/80.....	37
4.3.2	White Sand 30/70.....	39
4.3.3	White Sand 100 Mesh.....	41
4.3.4	ULW 30/80.....	44
4.4	Detailed Discussion.....	49
4.4.1	Experiment Limitations.....	49
4.4.2	Conventional Proppant in SRV.....	50
4.4.3	ULW Proppant in SRV.....	52
4.4.4	Cluster Proppant Pack.....	55
CHAPTER 5 NUMERICAL MODELING OF CLUSTERED PROPPANT.....		56
5.1	Model Setup.....	56
5.2	Simulation Example.....	56
5.3	Discussions.....	60
CHAPTER 6 CONCLUSIONS AND FUTURE WORK.....		62

6.1	Conclusions .....	62
6.2	Future work .....	62
	REFERENCE.....	64
	APPENDIX A.....	68

## LIST OF FIGURES

Figure 2.1 Microseismic fracture mapping shows complex network growth in shales.....	7
Figure 2.2 Stress-dependent conductivity of different proppants.....	9
Figure 2.3 Fractures used for conductivity tests.....	10
Figure 2.4 Measured aperture distributions for a single fracture from a coal core sample. ....	13
Figure 2.5 FracBlack HT ULW proppant, 14/40 mesh.....	15
Figure 2.6 ULW proppant transportation test.....	16
Figure 2.7 Illustration of how HiWay frac creates clustered proppant pack to improve conductivity.....	18
Figure 2.8 “HiWay Fracturing Simulation”.....	18
Figure 3.1 Flow chart of experiment procedure.....	20
Figure 3.2 Niobrara outcrop view.....	21
Figure 3.3 Core preparation before test.....	22
Figure 3.4 Placement patterns of proppants.....	22
Figure 3.5 Proppant types used in tests.....	23
Figure 3.6 CMS-300 permeability test machine.....	24
Figure 3.7 Geometry model of two test methods.....	25
Figure 3.8 Stress conditions comparison.....	26
Figure 4.1 Naturally fractured shale sample.....	31
Figure 4.2 Permeability versus confining stress for naturally fractured shale sample.....	32
Figure 4.3 Shear opened shale sample.....	33

Figure 4.4 Saw-cut versus sheared fracture permeability. ....	34
Figure 4.5 Saw-cut fracture permeability before and after proppant test. ....	35
Figure 4.6 Conventional proppant before and after test at 0.005 lb/ft <sup>2</sup> concentration. ....	36
Figure 4.7 LWC 40/80 propped fracture permeability versus confining stress. ....	38
Figure 4.8 LWC 40/80 fracture permeability versus proppant concentration.....	39
Figure 4.9 White sand 30/70 fracture permeability versus confining stress.....	40
Figure 4.10 White sand 30/70 fracture permeability versus proppant concentration. ....	41
Figure 4.11 White sand 100 mesh fracture permeability versus confining stress.....	42
Figure 4.12 White sand 100 mesh permeability versus proppant concentration. ....	43
Figure 4.13 Fracture permeability versus proppant concentration for different proppant types at 5000 psi confining stress. ....	44
Figure 4.14 ULW 30/80 saw-cut fracture permeability versus confining stress.....	45
Figure 4.15 ULW 30/80 propped saw-cut fracture permeability versus proppant concentration.....	46
Figure 4.16 ULW 30/80 Fracture permeability versus confining stress in sheared fracture. ..	47
Figure 4.17 ULW 30/80 fracture permeability versus proppant concentration in sheared fractures.....	48
Figure 4.18 ULW 30/80 fracture permeability versus proppant concentration in both sheared and saw-cut fracture at 5000 psi confining stress. ....	48
Figure 4.19 Embedment effect for fractures tested.....	53
Figure 4.20 Fracture roughness effect. ....	55
Figure 5.1 Model setup for clustered proppant simulation. ....	57
Figure 5.2 Domain of flow field and solid mechanics.....	57

Figure 5.3 Simulation results for disordered pillar placement and random pillar placement at 2000 psi confining.....	59
Figure 5.4 Normalized permeability versus confining stress with different proppant types and placement patterns.....	60
Figure A.1 Schematic of infinitesimal area calculation for loose and tight monolayer placement. ....	68
Figure A.2 Schematic of how size range effect concentration calculation. ....	69
Figure A.3 Proppant sample sorting device. ....	70

## LIST OF TABLES

Table 3.1 Estimated critical monolayer concentration range for proppants used. ....	28
Table 3.2 Test arrangement. ....	28
Table 4.1 Permeability test result of the naturally fractured shale sample. ....	32
Table 4.2 Permeability test result of opened fractures. ....	33
Table 4.3 Fracture permeability before and after used. ....	35
Table 4.4 Color and proppant concentration relationship. ....	36
Table 4.5 Permeability test result for LWC 40/80. ....	38
Table 4.6 Permeability test result for white sand 30/70. ....	40
Table 4.7 Permeability test result for white sand 100 mesh. ....	41
Table 4.8 Permeability test result for ULW 30/80 in saw-cut fractures. ....	44
Table 4.9 Permeability test result of ULW 30/80 in sheared fractures. ....	46
Table 4.10 Ratio of tested concentration to critical monolayer concentration for different proppant types. ....	51
Table 5.1 Assumed solid mechanics properties pillars and shale rock. ....	58
Table 5.2 Pressure difference between two ends for different placement pattern and pillar solid mechanics. ....	58

## ACKNOWLEDGEMENTS

I would like to express the deepest gratitude to my advisor, Dr. Hazim H. Abass, for his great support throughout this work. Special thanks are to Dr. Azra N. Tutuncu, for her suggestions and help, and to Dr. Jennifer L. Miskimins for her inspiring discussions and corrections to this work.

I have to thank FAST consortium members for the financial support for this project and the valuable suggestions from every consortium meeting.

Additionally, I am thankful to Joe Chen and Al Sami for their help and instructions to the lab experiments.

I am thankful to Denise Winn-Bower and Terri Snyder for every kind support they provided.

I would like to thank Dr. Zhao-qin Huang for his help in software modeling and thank every friend and colleague who has discussed this research with me and inspired me with new ideas.

I am thankful for all the support from my family.

## CHAPTER 1

### INTRODUCTION

The success of shale resource exploitation during the past several years has been mainly due to the evolutionary development of hydraulic fracturing techniques. The two most well-known innovations in hydraulic fracturing design are the multistage fracturing technique and water fracturing fluid system. It is believed that, via the above two techniques, complex fracture networks are created in fractured shale plays to make low permeable formations productive. The concept of Stimulated Reservoir Volume (SRV) has been used to describe such fracture networks (Mayerhofer et al. 2010).

Despite the booming shale revolution, almost all wells in shale plays show rapid decline after a short period of production (EIA 2014). The closing of fracture networks because of various damage mechanisms is believed to be one of the major reasons for this decline (Vincent and Besler 2013). The study of the SRV collapse involves studying several types of fractures: 1) fractures that naturally exist in shale formations; 2) fractures that are created during hydraulic fracturing operation and are closed after the operation; and 3) fractures that are propped by proppant after fracturing. All of these types of fractures may be connected during hydraulic fracturing and create a flowing SRV system. The closing of any part of the system is a reason for production decline. Much research has been done on this topic, yet there are many aspects that are not well understood by the industry.

Beyond the complexity of the study of an SRV system in shale plays, the development of new proppant products and fracturing techniques keeps refreshing our understanding and brings new ideas to the industry. Some of the innovations have already shown positive field

response and have potential to further improve the effect of hydraulic fracturing to the industry. Thus, study of the possible effects of these novel products and techniques to the SRV system is also warranted.

This thesis focuses on lab stress sensitivity tests of permeability in different stages of shale fracture systems, primarily the space where fractures are not sufficiently propped by proppant. New fracturing techniques and proppant products are also considered. Through arranging tests with different combinations of proppant type, proppant concentration, proppant placement pattern and fracturing techniques, needed information on the contribution of insufficiently propped fractures to the overall productivity of hydraulically fractured shale well is provided. Experimentally based correlations are provided to improve the development of hydraulic-fracture modeling of unconventional wells.

## **1.1 Research Objectives**

The objectives of this thesis were as follows:

- To test the stress-dependent property of four different kinds of proppant with low proppant concentration. Tests were done in natural and induced fractures in Niobrara shale core samples. Proppant type considers ultralight weight proppant (ULW 30/80), lightweight ceramic (LWC 40/80), white sand 30/70 and white sand 100 mesh.
- To use different placement patterns to simulate proppant performance in shale SRV systems for each proppant type. Patterns include well propped partial monolayer, poorly propped partial monolayer and clustered proppant pack.
- To use different proppant concentrations to analyze their effects on overall conductivity distribution for each proppant type. Testing results of lab proppant transportation in a

complex fracture system are considered.

- To build a simple numerical model that is flexible enough to be modified for various proppant analysis purposes.

## **1.2 Research Motivations**

Beside the main fractures that are usually propped by a multilayer proppant pack, there are large areas inside of an SRV system that, by logic, are not well propped by proppants. The contribution of these areas in SRV in shale plays has not been well studied. The conductivity performance of a proppant pack in these areas could be a reason for steep production decline in the early stage in shale plays. Since the laboratory multilayer proppant pack conductivity test is well accepted as an analogue of proppant behavior in the main fractures of fractured wells, a low to ultralow concentration proppant pack conductivity test is used to represent a poorly propped fracture area in this research.

ULW proppant and clustered type fracturing are two techniques that could possibly improve our fracturing techniques. Some lab research has already been done for these two topics. This research gives an overview of the availability and credibility of these techniques.

## **1.3 Research Contributions**

The conductivity distribution of four conventional proppants was studied from ultralow proppant concentration to low proppant concentration. The stress sensitivity of ultralight weight proppant is studied. Its optimal concentration value of conductivity performance is found. The high performance of clustered proppant pack is observed in lab and a numerical model is built to study its flow pattern in different in-situ stress conditions.

The results contribute to:

- Completing our understanding of conductivity distribution in a hydraulically fractured SRV system.
- Optimizing the application of ultralight weight proppant.
- Studying the flow patterns of clustered proppant pack in a small scale, through manipulating proppant placement pattern recommendations can be provided for field operation.

## CHAPTER 2

### LITERATURE REVIEW

In order to design practical and meaningful lab tests to correlate with real fracture systems in shale plays, especially when many systematical proppant tests have already been done by companies like Core Lab, one must: 1) use well-known concepts that have solid theoretical foundations or field response; 2) use relevant tests that bring novel ideas to conventional cognitions; and 3) consider new techniques that help design fracturing treatments.

#### **2.1 Water Fracturing in Shale Plays**

Hydraulic fracturing technology was first developed in the 1940s, and has increased dramatically since 2003, resulting in the successful exploitation of shale reserves (EEC Environmental 2010). Today, it is widely used in extraction of both conventional and unconventional reserves. Forecasts predict that more than seventy-five percent of natural gas development in the U.S. will rely on hydraulic fracturing in the future (American Petroleum Institute 2012).

Motivated mainly by cost savings and inefficient cleanup of traditional gel systems in unconventional formations, operators switched their focus to “waterfracs” at the beginning of the twenty-first century (Palisch et al. 2010). With the increasing understanding of unconventional resources like shale plays, waterfrac, which has got quite positive response in field applications (Palisch et al. 2010), is obtaining justification from the academia. In these unconventional formations where waterfracs are frequently used, the fracturing fluid – usually slickwater, linear gel or water with additives, is not as cohesive and strong as conventional crosslinked gel system. In addition, fracture width is usually smaller with low proppant

concentrations. However, the scale of waterfracs is generally immense. A tremendous amount of water is pumped during a stimulation operation and pumping time can exceed six hours (Palisch et al. 2010). On the one hand, low friction fracturing fluid and high pump rates help fractures propagating to a big volume of formation rock with complex geometry consisting of main fractures, secondary fractures, induced fractures and connected natural fractures. On the other hand, a large amount of proppant can be carried into these systems, and then settle in a complicated configuration.

Generally, 30/70 mesh and 100 mesh sand are considered to be economical in these massive hydraulic fracture operations. 20/40 sand and 40/80 lightweight ceramic are potential options in “tail-in” process (Coulter et al. 2004).

## **2.2 Stimulated Reservoir Volume**

SRV was brought to the industry in the early 2000s to explain the booming recovery of fossil fuels from shale plays (Mayerhofer et al. 2010). Observations from microseismic events show that hydraulic fracture in shale formations seemingly touches more areas than has been conventionally considered. See Figure 2.1. Following this observation, SRV theory and reservoir models were developed. However, SRV developed from microseismic gradually shows defects as microseismic monitoring is incapable of capturing the P-wave caused by rock failure and the placement of geophones (Cipolla and Wallace 2014). In addition, as a reverse interpretation process, microseismic mapping has certain accuracy and precision limits. Field infill drilling and production data have proven that microseismic data needs to be carefully understood (Vincent and Besler 2013).

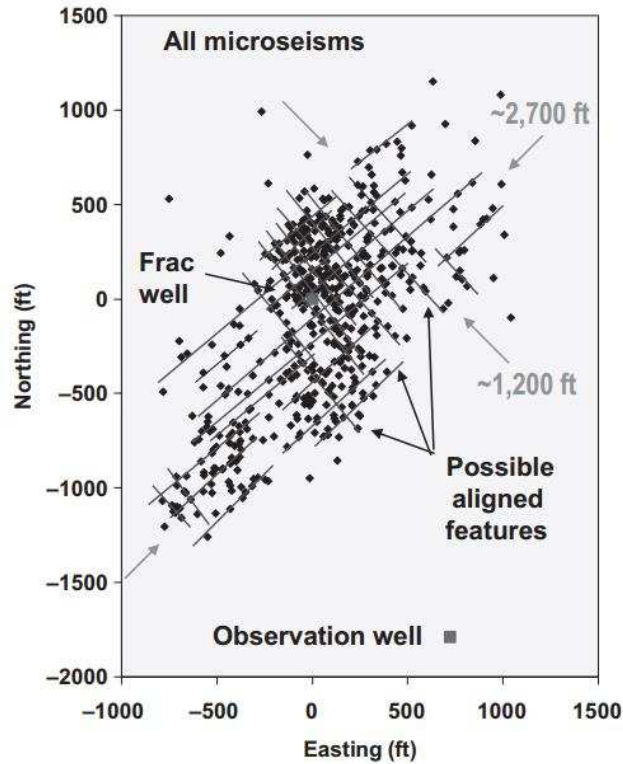


Figure 2.1 Microseismic fracture mapping shows complex network growth in shales (Mayerhofer et al. 2010).

Field mine back experiments are used to show the geometry of fractures in shallow formations. However, in shale hydraulic fracturing, there is no direct evidence so far capable of convincing us of what the fracture exactly looks like. Yet, through combining comprehensive evidence, a fractured “volume” of formation is the most logical explanation. Despite discussions about how this “volume” should be obtained and matched with fracture modeling and reservoir simulation (Cipolla and Wallace 2014), the fact that hydraulic fracturing has been shocking the rocks and creating a complex fracture system before production in low permeable shales is well accepted.

### 2.3 Stress Dependent Conductivity

Reservoir and fracture systems could be sensitive to different factors. One of the most dominant ones is in-situ stress. The fact is that a rock formation is compressed by overlaying

formations and in-situ effective stresses-the actual stress that exerts on rock skeleton, change with the decrease of pore pressure during production, which is illustrated by the equation below.

$$\sigma' = \sigma - \alpha p \quad (2.1)$$

In which  $\sigma'$  stands for effective stress in psi;  $\sigma$  stands for total stress in psi;  $\alpha$  stands for Biot's coefficient, a value between zero and one; and  $p$  stands for pore pressure in psi.

This equation was originally developed by Terzaghi's (1925) study on soil skeleton without the coefficient  $\alpha$ , and was then modified by Biot (1941), who considered the porous structure of undersurface rocks, claiming that with different rock types, pore pressure could partially take up the total stress at different percentage; this percentage is Biot's coefficient. Usually the empirical relationship between porosity and Biot's coefficient is used to estimate its value.

The permeability sensitivity of formation rock due to pressure change was tested by Davies and Davies (2001). Results show that for rocks of the same rock type with little bury depth difference, the permeability decline with increasing net effective stress has huge variation. There is no unique relationship between permeability and in-situ stress (Davies and Davies 2001). The only way to quantitatively analyze the stress sensitivity of formation rock is with a lab test.

Similar to rock formation, fracture permeability change with different stress can only be tested in a lab. Cylindrical saw-cut core samples were used to test fracture permeability sensitivity of different rocks (Cho et al. 2012; Tian 2014, etc.). In these tests, ideal smooth cut fractures were assumed to be analogous to the unpropped fracture underground.

For propped fractures, stress dependent conductivity tests of different proppants are

analogues of main fracture stress sensitivity. See Figure 2.2. Stim-lab started its proppant consortium in 1986. Numerous conductivity tests have been done considering comprehensive damage mechanisms. Based on these data, the production prediction simulator, Predict-K was established. The analysis of the conductivity tests is embedded in the fracture modeling software.

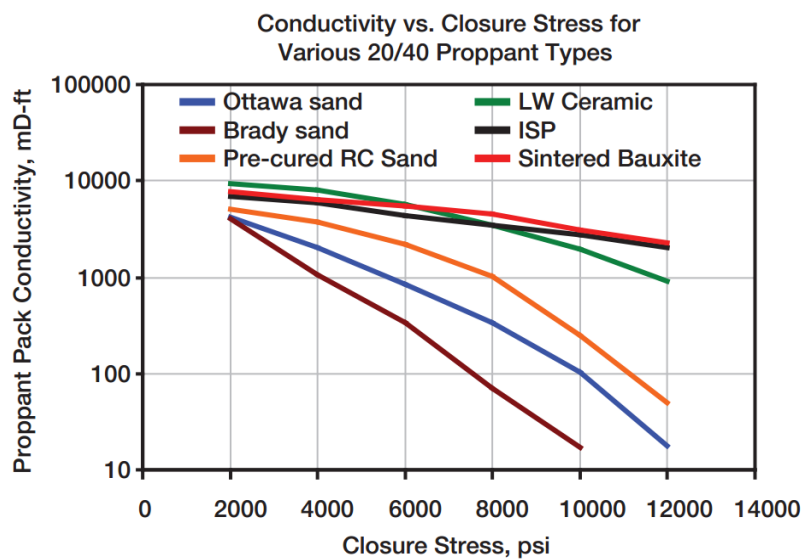


Figure 2.2 Stress-dependent conductivity of different proppants (Economides 2007).

Eighty-eight tests of the hydraulic fracture conductivities of Barnett shale were conducted by Kamenov et al. in 2013. In these tests, outcrop rock samples were collected from a quarry and were cut to fit into the API conductivity cell. Three types of fractures: natural fracture, aligned fracture and displaced fracture were tested in both unpropped and propped conditions. See Figure 2.3. One hundred mesh, 40/70 mesh and 30/50 mesh sand were used as the fracturing proppants at mainly four concentrations: 0.03 lb/ft<sup>2</sup>, 0.06 lb/ft<sup>2</sup>, 0.1 lb/ft<sup>2</sup> and 0.15 lb/ft<sup>2</sup>. Here 0.06 lb/ft<sup>2</sup> is considered to be the full monolayer concentration for 100-mesh sand.

The fractures used in this cited research were created by opening the highly laminated bedding plane of Barnett outcrop. The focus was on the properties of fractures rather than

proppant performance in harsh conditions. Thus, comparisons between different types of fractures with different proppant sizes were provided qualitatively.

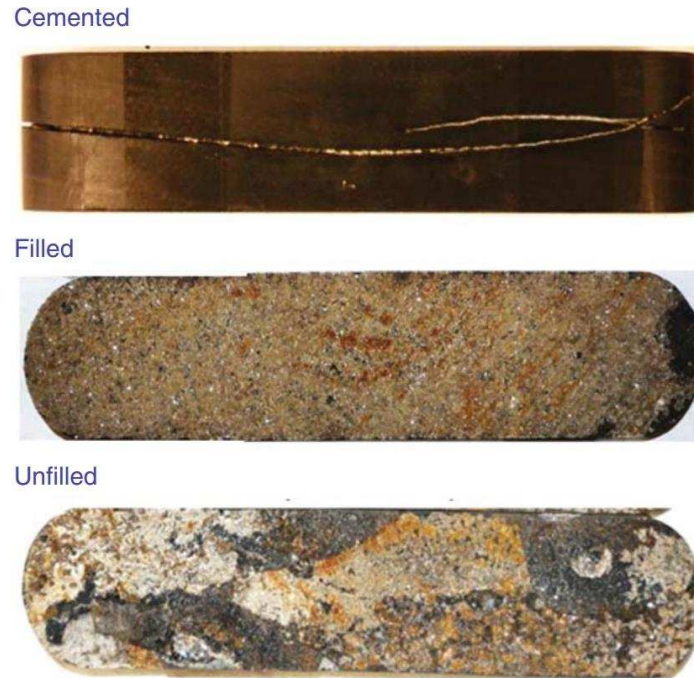


Figure 2.3 Fractures used for conductivity tests (Kamenov et al 2013).

In all of these cited researches, permeability changes with increasing effective confining stress. For the matrix, the stress sensitivity could be explained by the Kozeny-Carman equation (Chapuis and Aubertin 2003):

$$k = \frac{\phi r^2}{8\tau^2} \quad (2.2)$$

Where  $\phi$  is porosity;  $r$  is pore radius, and  $\tau$  is tortuosity. With increasing confining stress, tortuosity barely changes, porosity changes slightly and pore radius changes a lot.

For an unpropred fracture, using an equation derived from cubic law can improve our understanding of the sensitivity of fracture permeability, the equation is expressed as (Sarkar et al. 2004):

$$k_f = \frac{w_f^2}{12} \times 10^9 \quad (2.3)$$

Where  $k_f$  stands for fracture permeability in millidarcies, and  $w_f$  stands for fracture width in millimeters. This equation shows fracture permeability has a second order relationship with fracture width. After hydraulic fracturing, when in-situ stresses close fractures with time, fracture permeability will decrease.

For a propped fracture, the industry focus was on the proppant pack conductivity test. In the real world, propped fracture permeability degradation is a rather complicated problem, even if the problem is shrunk down to the factors that only relate to stress. Firstly, proppant has a certain roundness and sphericity level. This geometry property directly leads to uneven stress distribution in the proppant pack with different confining stresses. Secondly, the packing process during a proppant conductivity test makes permeability a dependent variable versus an intrinsic property of the proppant pack. A standard deviation of +/- 10% is often observed in lab tests (Barree et al. 2003). The third is the interaction between proppant and rock plate surface. The proppant pack goes through initial packing, compaction, compression and probably failure. The damage factors that can be well analyzed through lab experiments include (Duenckel et al. 2012):

- Mechanical failure (reservoir fluid and temperature condition)
- Proppant embedment
- Formation fines migration
- Formation spalling
- Fracturing fluid damage
- Stress cycling

- Asphaltene deposition
- Proppant dissolution

Not all of the factors are required by industry standards like *ISO 13503-5*, yet they are well known by the industry and considered by proppant companies. Almost all of the damage factors are stress-related. However, there are other damage factors that are still difficult to measure at lab scale yet could have an impact on proppant pack conductivity in the real world (Barree et al. 2003):

- Non-Darcy flow effect
- Multiphase flow
- Multiphase non-Darcy flow
- Gravity and viscous segregation
- Reservoir flow capacity

All of the factors mentioned above could be cumulative; if they are all considered, the fracture conductivity in the real world must deviate dramatically from the clean pack baseline data. A result in the fracture simulation is a really smaller number of effective half-length than the opened half-length.

In addition, the industry has increased its focus on the effects of rock mechanics (Jansen et al. 2015, Zhang 2014) and fracture surface topology (Pyrak-Nolte and Morris 2000) to fracture conductivity. See Figure 2.4. These factors are usually not considered in an ideal lab conductivity test.

All of the aforementioned aspects explain the sensitivity of fracture permeability and its

complexity.

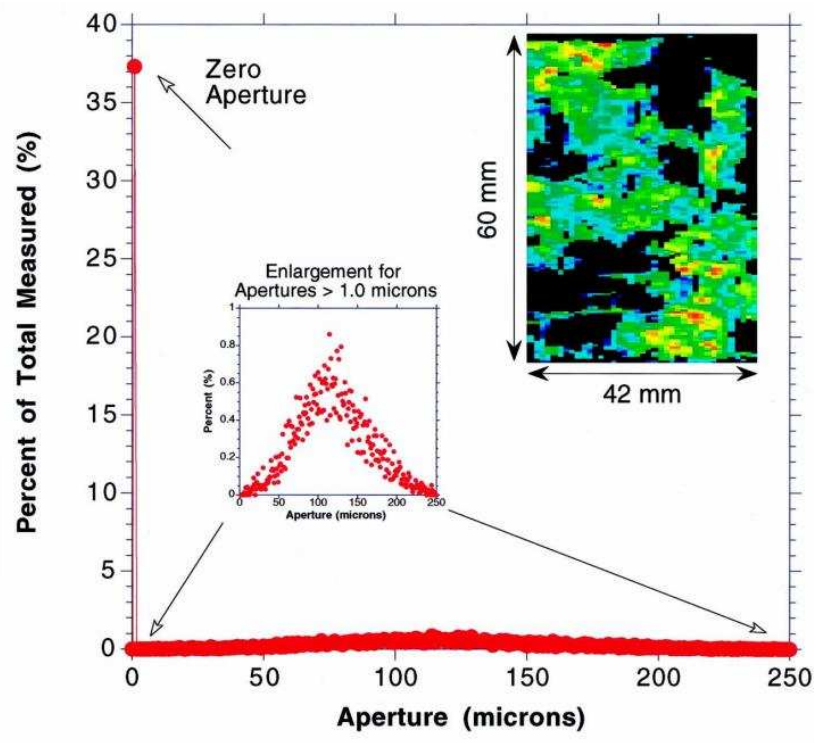


Figure 2.4 Measured aperture distributions for a single fracture from a coal core sample (Pyrak-Nolte and Morris 2000).

## 2.4 Fracture Effectiveness

Irrefutable evidence has shown hydraulically-propped fractures collapse during production. This is against most reservoir simulation assumptions. Vincent and Besler (2013) have worked to improve public understanding of hydraulic fracturing in unconventional resource plays. It is stated that field evidence has indicated that fracture effectiveness and its durability should be more focused. For example, infill drilling touched near virgin zone covered with microseismic swarm during previous fracturing; the interference between fracture-connected wells declines severely after 6 months of production; such interference is really weak between the well-connected wells at the beginning of production; decline curve is generally steeper than initial expectations (Vincent and Besler 2013).

Apart from the effects of geology and reservoir characteristics, these field observations indicate that the industry conductivity test still needs improvement, especially with increasing number of new proppant products and fracturing techniques being developed.

## **2.5 ULW Proppant**

ULW proppant has been considered recently by many operators, and has been studied by different lab tests (Brannon et al. 2004; Brannon et al. 2009; Gaurav et al. 2010; Trujillo et al. 2011). *Sun Drilling* is the company that manufactures the well-known nanocomposite ULW. Now they have FracBlack HT proppant as the third generation of this ULW product. Lab tests and field applications have shown positive results on these products. See Figure 2.5.

Current applications include:

- supplemental use with sand
- replacement for sand – 100 mesh
- partial monolayer
- acid fracs

Could be applied in:

- slick water
- traditional frac fluid
- waterless fracture stimulation applications
- gravel packs

The most current application is the supplement of conventional proppants. ULW is pumped with sand or other proppant. Lab proppant transportation tests have shown that a) ULW, with its apparent specific gravity close to water, could ‘float’ and occupy the upper and deeper

position of the opened fracture; b) in both static and dynamic conditions, the ULW are easier to be carried by fluid; c) ULW could also help to move the top of sand dune to move forward; d) all of the ULW proppants are taking the fracture in a partial monolayer pattern. See Figure 2.6.



Figure 2.5 FracBlack HT ULW proppant, 14/40 mesh.

Another systematic test (Gaurav et al. 2010) has shown that this ULW product has Young's modulus close or even smaller than walnut hull. It is highly deformable, yet it has high stress resistance. It tends to stay intact and simply becomes flattened instead of being crushed at high pressure. Thus, the fact that ULW proppant has different failure behavior comparing with conventional proppant and the fact that ULW proppant has potential to occupy higher side of fractures in SRV are like a drawback and an advantage that should both be considered.

## **2.6 Partial Monolayer**

The concept of partial monolayer is highly related to the concept of ULW proppant. Darin and Huitt (1959) suggested that proppant with a partial monolayer pattern in a fracture could provide high conductivity due to the void space between each particle. Initially, a partial monolayer was examined and was considered difficult to achieve in the field (Howard and Fast

1970).



(a)



(b)

Figure 2.6 ULW proppant transportation test: (a) static condition; (b) dynamic condition (Youtube 2012).

The reasons that a partial monolayer was not looked upon favorably were mainly from the conventional hydraulic fracturing perceptions (Brannon et al. 2004). However, in modern unconventional hydraulic fracturing, sheared fractures and connected natural fractures that far away from the wellbore could only open at a limited width and would only be poorly propped by proppants. In addition, development of ULW, as discussed previously, at least in lab test level, shows mainly a partial monolayer placement pattern. These reasons justified the refocus of the study on fractures with partial monolayer proppant.

One type of ULW proppant, ULWP-1.25 has been tested and compared (Brannon et al.

2004). The test included a transportability and partial monolayer conductivity test. The proppant mesh sizes considered were 8/16, 12/20, 20/40, and the minimum proppant concentration considered was 0.03 lb/gal. It was concluded that ULW proppant has potential to be successfully used in the real world.

## **2.7 Clustered Proppant Fracturing**

Several companies have developed similar techniques to create an infinite conductivity channel in fracturing. For example, HiWay Flow-Channel fracturing technique from Schlumberger and Pillar-type fracturing from Halliburton. It has been claimed that field applications have proven their potential for water savings and production improvements. Due to different injection pulses of proppant/fiber laden fracturing fluid, it has been hypothesized that a clustered proppant pack will be created within the created fracture domain so that infinite conductivity paths are generated which provide much more conductivity compared to conventional proppant packs. See Figure 2.7. Lab proppant transportation tests and clustered proppant conductivity test have been conducted (Medvedev et al. 2013) to simulate field pumping process, proppant pack geometry and proppant pack stress conditions. See Figure 2.8. Similar work was done by Halliburton (Inyang et al. 2014) based on their own spacer fluid and proppant-aggregate-laden fluid. In this system, an agglomerating agent is used to keep the proppant bonded together during fracturing, which works as the fiber system in HiWay Flow Channel fracturing. In addition, Weatherford has tried to build numerical models for clustered proppant hydraulic fracturing from flow simulation to fracture conductivity maps and then production forecasting (Huang et al. 2015).

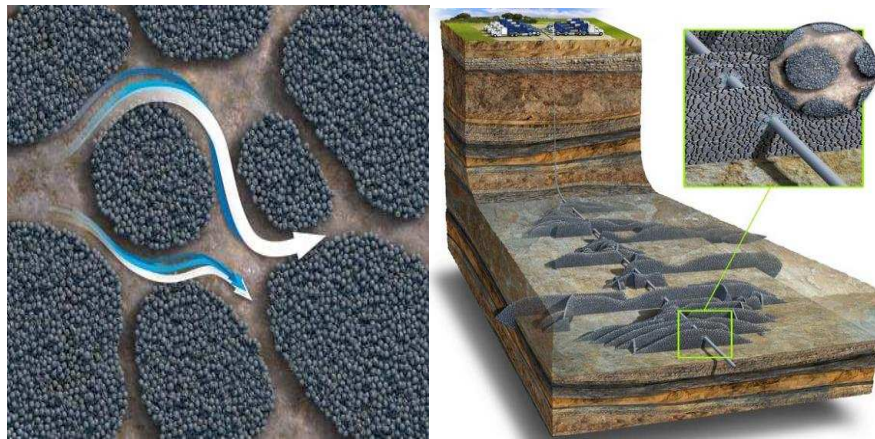


Figure 2.7 Illustration of how HiWay frac creates clustered proppant pack to improve conductivity (Schlumberger 2015).

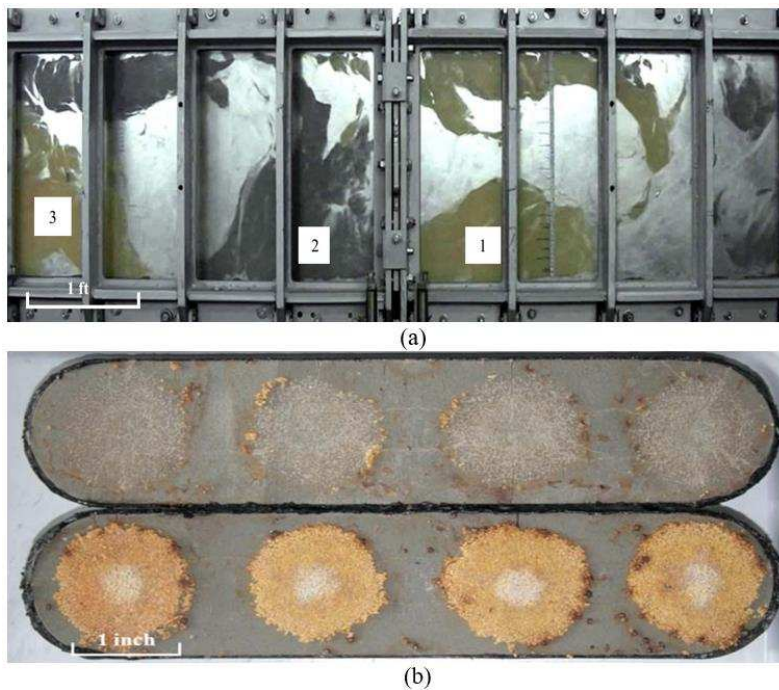


Figure 2.8 “HiWay Fracturing Simulation”: (a) Proppant transportation simulation; (b) Proppant pack conductivity test. (Medvedev et al. 2013)

## 2.8 Summary

The SRV in shale plays is sensitive to in-situ stresses, no matter the fracture network is propped or unpropped by proppant; a collapsing fracture is a side evidence of SRV stress sensitivity. Proppant pack with concentration below monolayer has been discussed and studied, yet some concentrations and new types of proppant have not been covered; ULW has potential

to occupy the upper side of the opened fracture areas that conventional proppant by its nature can hardly touch; clustered proppant pack can increase fracture efficiency.

Inspired by the aforementioned studies, this research focuses on:

- Low concentration proppant test for conventional proppants. The proppant types considered in this research are white sand and lightweight ceramic (LWC). The low concentration proppant pack for these types of proppant is generally created at the tips of fractures where fracture width is small and the position is far away from wellbore. From a fracture modeling point of view, if the damage mechanisms are considered, these areas can definitely be cut off away from the effective half length. Yet, it is meaningful to see how this small amount of proppant can make changes to the overall fracture conductivity distribution.
- Low concentration proppant test for ULW proppant. Lab proppant transportation has proven that partial monolayer proppant pack of ULW proppant can be achieved on the upper side of fractures. There is still no data showing what the concentration range of this partial monolayer proppant pack is. A complete permeability analysis ranging from zero to monolayer concentration can bring inspiration to later research.
- The potential of clustered proppant pack. This topic is also highly related to a proppant transportation test as the exact placement pattern of the clustered proppants has to be well understood before any conductivity test. This research will do tests based on a very basic placement pattern and try to build a model that can be modified for the analysis of any kind of placement pattern.

## CHAPTER 3

### LABORATORY EXPERIMENT

This research bears the complexity of fracture system in shale fracturing and proppant placement pattern and focuses on their impacts on fracture conductivity. In addition, ULW, and cluster proppant placement technique, are also considered. This section will detail the experiment process, equipment and method.

#### 3.1 Research Plan

The flow chart of how this research was conducted is shown in Figure 3.1. First, rock samples from an area near Boulder that has been identified as Niobrara shale formation were collected. The way this kind of shale sample contains fossil fuel inside, its ultra-tightness and easy accessibility make it perfect for lab testing. Cores with natural fractures or cores manually fractured were used with different kinds of proppants to simulate proppant placement in a fractured shale formation.

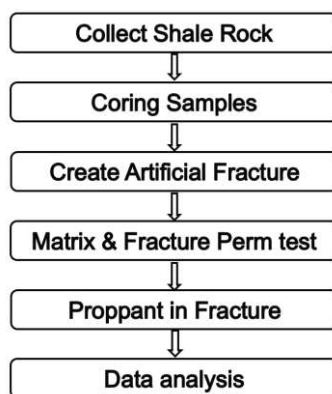


Figure 3.1 Flow chart of experiment procedure.

#### 3.2 Sample Preparation

Shale rock samples and conventional proppant samples were the bases of the tests in this research. The samples had to be feasible to get, representative of the in-situ condition, and

applicable for upscaling or field use.



Figure 3.2 Niobrara outcrop view.

The shale samples source is the outcrop of Niobrara shale from CEMEX quarry. See Figure 3.2. The Niobrara shale has been under exploitation since the 1920s, and now 20+ companies are involved in its development. Companies, such as EOG, have gained sufficient payback from shale oil in this area.

The next step was to preserve and core the samples to proper size. Coring and saw cutting were used to create artificially fractured core samples. The cores were all drilled vertically to the bedding planes. The matrix permeability tested in this research is only the vertical matrix permeability.

A diamond saw was used to create fractures from the cylindrical cores. The difference of vertical and horizontal permeability is not compared in this research. Two cores on a certain block were left intact to measure matrix permeability. Then fractured cores were wrapped with tape and put into the CMS-300 to measure fracture permeability. See Figure 3.3.

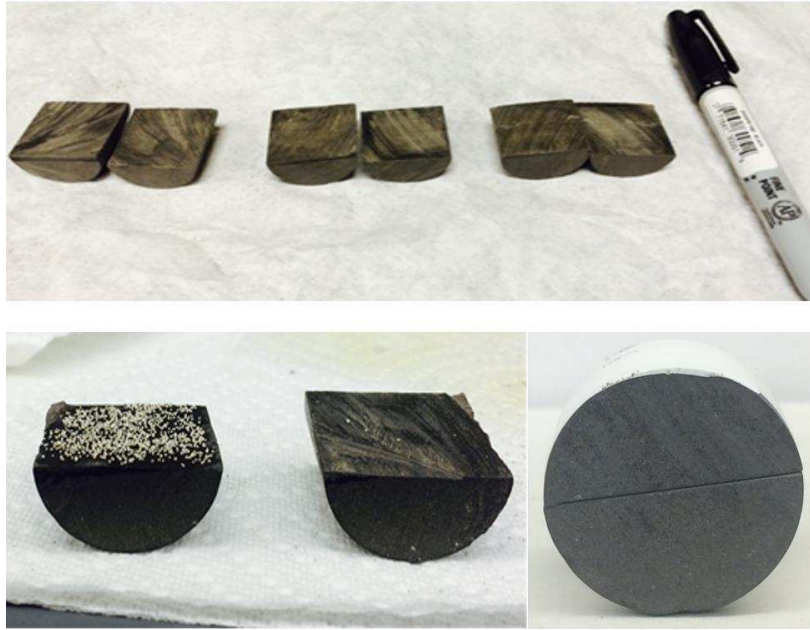


Figure 3.3 Core preparation before test.

Different types of proppants were placed on the fracture surfaces under different placement patterns. To keep the proppants on the fracture surface, a thin film of glue was put on the fracture surface. Then the glue was left to dry and Scotch tape or other kind types were used to wrap the core and keep the proppant inside the core. See Figure 3.4.

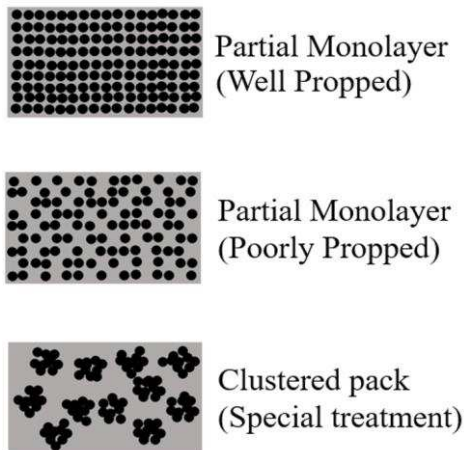


Figure 3.4 Placement patterns of proppants.

The placement patterns considered were well propped partial monolayer, poorly propped partial monolayer, and clustered pack. The proppant types considered were ULW proppant,

lightweight ceramic 40/80 (LWC), white sand 30/70 and white sand 100 mesh. See Figure 3.5.



Figure 3.5 Proppant types used in tests.

### 3.3 Test Equipment and Method

The CMS-300 Automatic Core Measurement was used; it is available for core samples with a permeability level as low as 10 nanodarcy. See Figure 3.6. The pore volume and Klinkenberg permeability could be determined during measurement. The confining stress was user-defined between 500 psi - 9800 psi, and the stress was applied in both radial and axial directions.

The pore volume was measured or assumed at first. Then the pressure transient “Blowdown” technique was used for permeability measurement. A tank of helium with accurate known volume was discharged through the core to the atmosphere. The pressure values on both ends were recorded with time to determine gas flow rate at any given time. The Klinkenberg permeability was measured. Combined with the slip factor, high velocity, and non-Darcy flow factors, the air permeability was determined. Such measurement was repeated at each confining stress so that the stress sensitivity of a certain core could be analyzed.

It should be mentioned that as the equipment uses “Blowdown” technique, the upstream helium pressure is usually about 190 psi to 230 psi while the downstream pressure is the ambient condition. The effective confining pressure of each step is around 100 psi lower than the preset confining pressure. This difference is ignored in this research. Each test was done with confining stress ranging from 1000 psi to 5000 psi, as this has been verified to be a safe range for the outcrop shale rock.

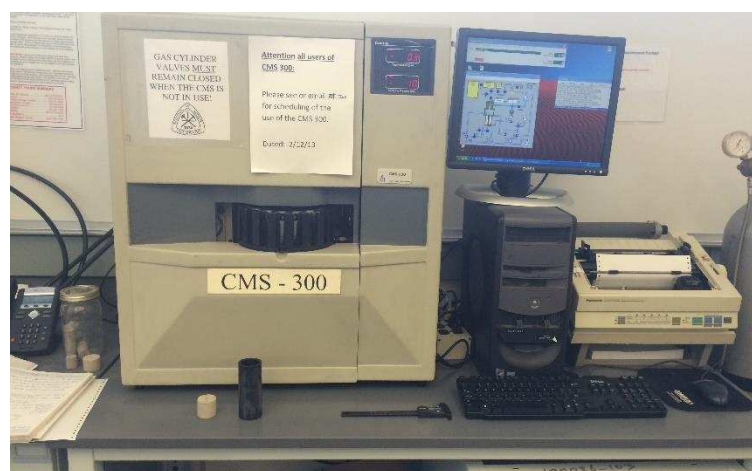


Figure 3.6 CMS-300 permeability test machine.

### 3.4 Verification of Test Method

For fracture permeability measurements, usually the API conductivity test cell is used. With fracture width manually measured during testing, conductivity value is obtained. However, such cells are not usually owned by a university, so as an alternative, researchers have used cut cylindrical cores that can fit into conventional permeability measurement equipment like CMS-300 to study fracture permeability. However, the credibility of such methods has not usually been studied. As stress is the main concern of this research, the comparison of stress distribution on proppant pack between CMS-300 and API conductivity cell was studied.

The COMSOL Multiphysics software was used. At first, the geometry model was built for both test methods. For CMS-300, a cylindrical core was cut in the middle to simulate the fracture in real test, and nine pillars were placed in the middle evenly on the fracture surface. For the API conductivity cell, two plates were used to simulate a conductivity cell. The exact nine pillars were placed at the same position on the fracture surface See Figure 3.7.

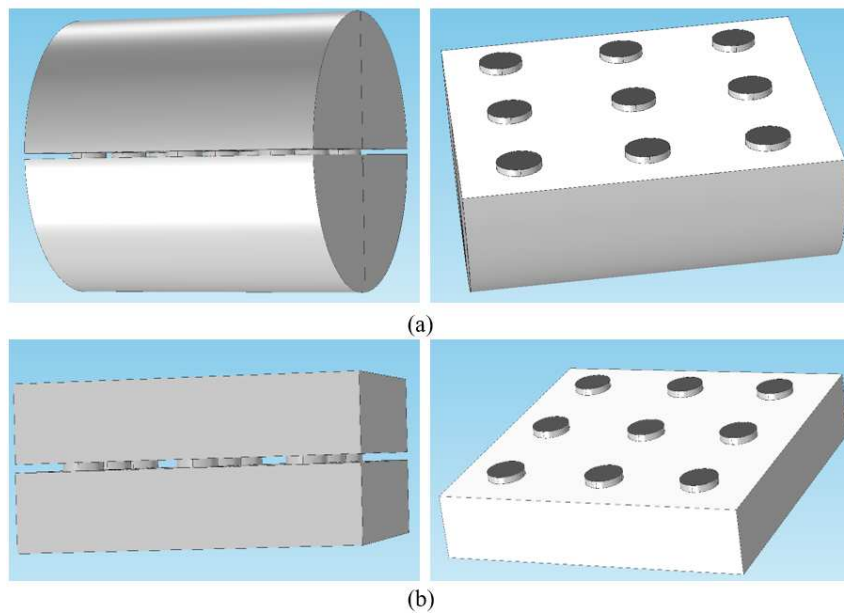
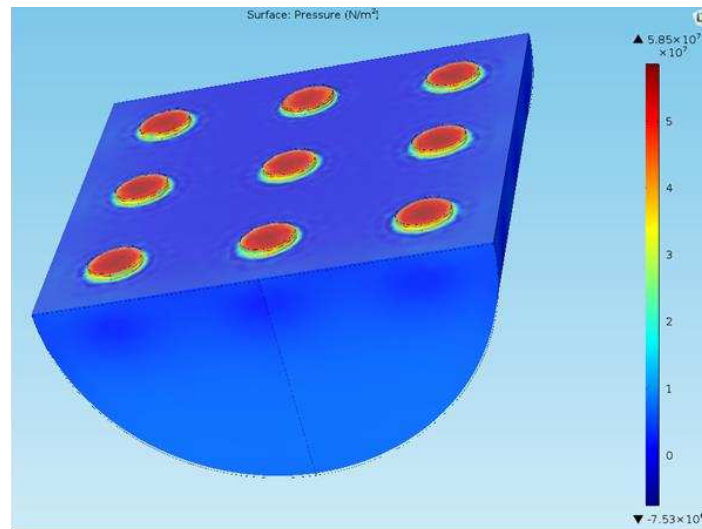


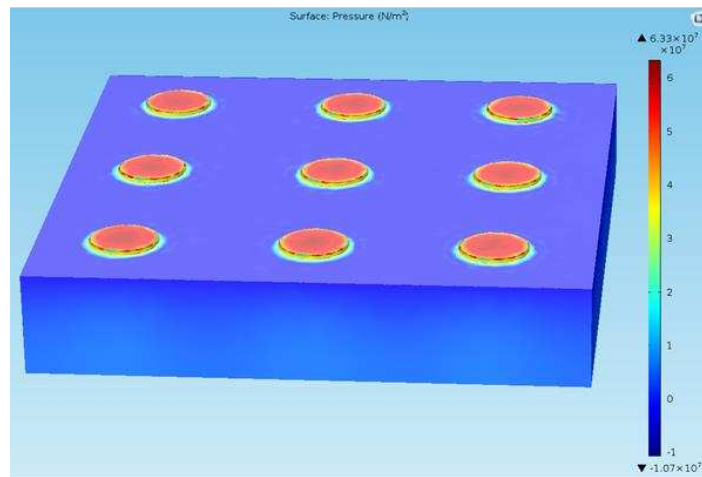
Figure 3.7 Geometry model of two test methods (a) model for CMS-300; (b) model for API conductivity cell.

Then the boundary conditions of both tests were defined based on the exact test conditions in the real world. Here  $8 \times 10^6$  Pa pressure was used for both cases. The rock Young's modulus was set to be equal to  $1 \times 10^8$  Pa. This low value has two concerns: 1) the deformation of proppant will be obvious 2) this value is actually very close to the documented Young's modulus of the ULW proppant sample used in this research. The finer mesh for finite element study was chosen to show better study results. The stress conditions for all the hypothetical proppants in those two geometry models are shown on the color legend on the right side of the graphic. See Figure 3.8.

The results show that in the middle of the pillar, the stress is more concentrated. In both tests stress on pillars is above  $5.5 \times 10^7$  Pa. The overall stress distribution is at the same level. The stress difference between these two models could be: for CMS-300, the whole cylindrical core is compressed from all directions; thus, the displacement of the middle point is more confined. For the conductivity cell, the proppant is just compressed in one direction.



(a)



(b)

Figure 3.8 Stress conditions comparison: (a) stress condition in CMS-300 test; (b) stress condition in conductivity cell test.

This study at least verified that for CMS-300 where the cylindrical core is used, the stress is evenly distributed on the fracture surface, and the stress level is exactly the same as the API

conductivity cell. With this in mind, the conductivity cell model (plate) is only used due to its simplicity in modeling.

### 3.5 Critical Monolayer Concentration

To simulate the poorly propped fracture, the critical monolayer concentration had to be determined first. The equation to estimate the minimum amount of proppant needed to form a full monolayer was derived by Brannon et al. (2004). The medium proppant sizes for ULW 30/80, white sand 30/70, and LWC 40/80 are respectively 0.027305 cm, 0.029718 cm and 0.024892 cm.

$$C_a = 5.20(1 - \phi)\gamma_p d_p \quad (3.1)$$

Where  $C_a$  stands for monolayer proppant concentration in lb/ft<sup>2</sup>,  $\phi$  stands for porosity,  $\gamma_p$  stands for proppant density in g/cc and  $d_p$  stands for proppant average diameter in inches.

Here a minimum obtainable porosity had to be assumed, and an average proppant diameter was estimated. These two “guesses” made this equation less practical to use. In addition, with a fracture that has a certain geometry, namely length, height and width, proppant diameter and proppant specific gravity should be the only independents to form a monolayer. Porosity here does not make much sense. A new equation to estimate this minimum concentration was derived, the expression is:

$$1.0724D\rho \leq C \leq 2.4766D\rho \quad (3.2)$$

Where  $D$  is proppant medium diameter in inches,  $\rho$  is proppant density in g/cc.  $C$  is critical monolayer concentration in lb/ft<sup>2</sup>. The detailed derivation is in APPENDIX A.

With the equation derived, the estimated critical concentration range calculated is shown in Table 3-1. The highlighted minimum monolayer concentration was observed to be a practical value in our lab test because when practicing the proppant placement process, it is almost

impossible to push all the proppants tightly together.

Table 3.1 Estimated critical monolayer concentration range for proppants used.

Proppant Type	Mesh Size	Medium Opening Size (inch)	Density (g/cm <sup>3</sup> )	Estimated Critical Concentration Range (lb/ft <sup>2</sup> )	
<b>ULW 30/80</b>	30/80	0.01075	1.054	0.031	0.071
<b>LWC 40/80</b>	40/80	0.0098	2.6	0.069	0.160
<b>White Sand 30/70</b>	30/70	0.0117	2.65	0.084	0.195
<b>White Sand 100</b>	100	0.0059	2.65	0.043	0.098

This information is really crucial in this research. For example, if the permeability contribution of a really small concentration of proppant needs to be analyzed, the ratio of its real concentration to critical monolayer concentration provides the quantitative view of this analysis. If two proppants of the same concentration need to be compared at the same confining stresses, their ratios to critical monolayer concentration are usually different.

Since ULW is one of the main focuses in this research, and previous tests on similar products have covered concentrations greater than 0.03 lb/ft<sup>2</sup>, in this research, 0.02 lb/ft<sup>2</sup> was set to be the maximum concentration value for most of the proppant products. The matrix for testing is listed in Table 3.2.

Table 3.2 Test arrangement.

Placement pattern	Proppant concentration (lb/ft <sup>2</sup> )			
	ULW 30/80	LWC 40/80	White Sand 30/70	White Sand 100
<b>Well Propped Partial Monolayer</b>	0.02	0.02	0.02	0.02
<b>Poorly Propped Partial Monolayer</b>	0.01	0.01	0.01	0.01
<b>Ultralow Proppant Concentration</b>	0.001 to 0.005	0.001 to 0.005	0.001 to 0.005	0.001 to 0.005
<b>Clustered Proppant</b>	0.01	0.01	0.01	0.01

With these tests, an overview of proppant performance at very low proppant concentration can be obtained. Beyond the tests listed in the matrix, some other tests are done for purposes,

such as analyzing the contribution of really low proppant concentration and refining concentration stages for optimal value. These will be discussed in later chapters.

## CHAPTER 4

### LABORATORY EXPERIMENT RESULTS

Permeability tests of different types of fractures were conducted step by step. The previously tested results were used as a reference for the results tested later. The test sequence was: 1) the permeability test of a shale sample with natural fractures in it; 2) the opened fractures (either saw-cut or sheared) that were used for proppant test, the permeability of this kind of fracture were tested ahead to compare with the naturally fractured sample and to be used as baselines for later proppant tests; 3) the permeability of fractures that were propped in a partial monolayer pattern. This kind of test contains various combination of proppant type, proppant placement pattern and proppant concentration.

#### **4.1 Naturally Fractured Shale Sample**

More than 30 tests have been done on various 1 inch and 1.5 inches cylindrical shale samples. Two kinds of fractures were used, including saw-cut fracture and sheared fracture. Four types of proppant were used, including: 30/80 ULW, 40/80 lightweight ceramic, white sand 30/70 and white sand 100 mesh. For the tests with proppant in fracture, the main focus was the decline pattern of each proppant type itself. The parallel comparison between proppant types should consider the fact that even if the absolute concentration value is the same, the ratios of these concentration values to their critical monolayer concentration are different.

The general matrix permeability of the shale blocks used in this research was tested by another PhD student (Cui 2015) and was found to be around tens to hundreds of nano-darcy. During the coring process of the shale blocks, a cylindrical core was obtained with natural fracture connecting both ends of the core. The permeability of this sample is tested using CMS-

300 as a comparison. It is also an example of the test result of all the permeability tests done on CMS-300.

It was only observed that this core is interconnected by natural fractures. It is difficult to quantify how many fractures contribute to permeability as what is inside of the core cannot be seen in this research. See Figure 4.1.

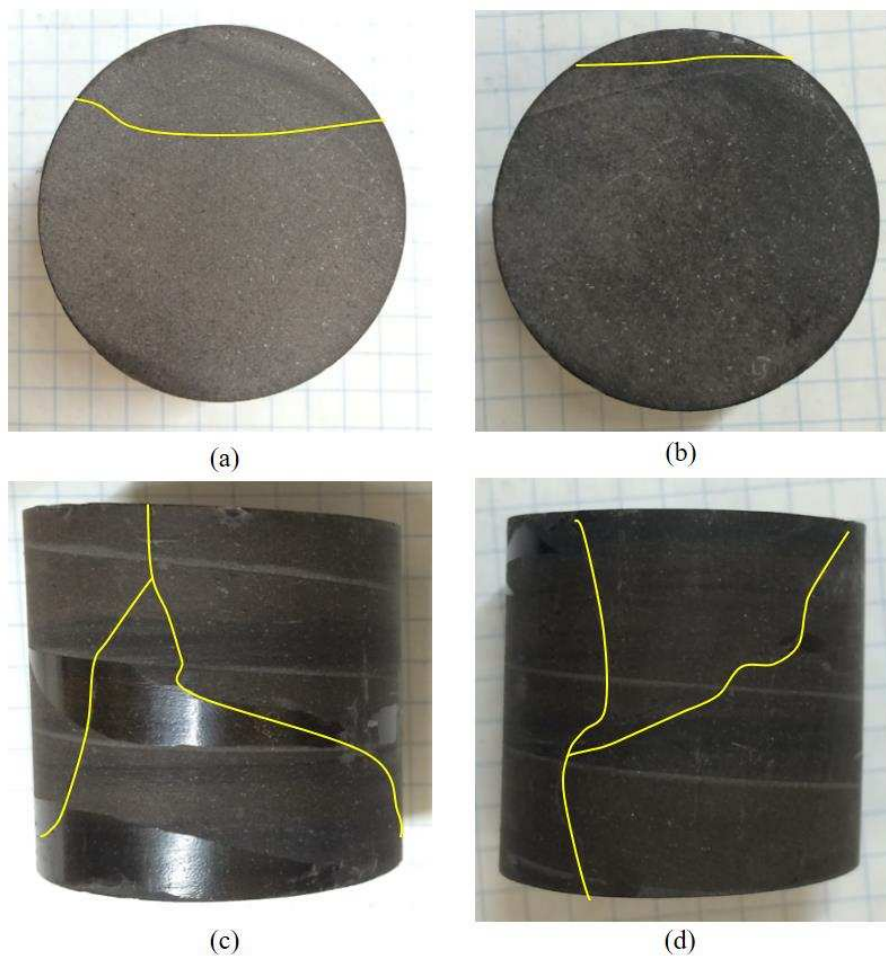


Figure 4.1 Naturally fractured shale sample: (a) top view (b) bottom view; (c) right side view (d) left side view.

Table 4.1 Permeability test result of the naturally fractured shale sample.

Confining Pressure (psi)	Naturally fractured core (md)
1000	4.32E-02
2000	1.19E-02
3000	5.32E-03
4000	2.89E-03
5000	1.56E-03

Figure 4.2 shows that the permeability of this naturally fractured core is between tens micron-Darcy to several micron-Darcy, which is about two to three magnitudes higher than the general matrix permeability. Permeability declines relatively fast between 1000 psi to 2000 psi confining stress and slows down between 2000 psi confining to 5000 psi confining stress.

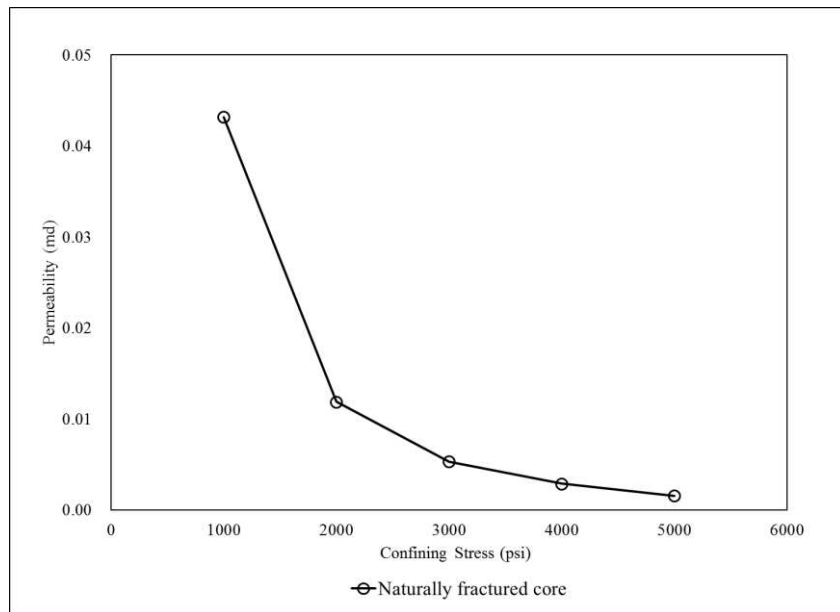


Figure 4.2 Permeability versus confining stress for naturally fractured shale sample.

In this research, the smoothness of this kind of decline curve is considered that a representative physical law is expressed. It is observed throughout all of the experiment that whenever experiment conditions are not well controlled, an irregular decline curve might be obtained. Namely, the absolute permeability value could be decreasing, but the data does not make much sense when plotted versus confining stresses. Every irregular test result required a

redo, and only the reasonable data is presented and discussed in this thesis.

## 4.2 Opened Fractures

Two types of fractures were studied: saw-cut fracture and sheared fracture. The saw-cut fracture was mostly used because of its easy accessibility. The fracture width was about 0.014 inches and core diameter was either 1 inch or 1.5 inches. Usually, the permeability of one or two saw-cut core samples from a shale block were tested to represent other saw-cut samples from the same block. Sheared fractures were obtained by chance and were used to verify the credibility of tests on saw-cut fractures as their fracture surface is closer to the fracture surface in the real world. Sheared fractures were used to test ULW proppant.



Figure 4.3 Shear opened shale sample.

At first, the permeability decline curves between these two types of fractures was compared in the same plot. See Figure 4.4. For the same fracture type, each permeability value was not distinguished between others as this plot is to show the permeability range of each fracture type and to compare the general scale difference between these two types of fractures.

Table 4.2 Permeability test result of opened fractures.

Confining Pressure	Saw-cut Fracture #1	Saw-cut Fracture #2	Saw-cut Fracture #3	Sheared Fracture #1	Sheared Fracture #2
1000	2.31E+00	3.43E+00	1.07E+01	2.08E+00	5.93E+00
2000	1.32E+00	1.27E+00	6.06E+00	1.10E+00	
3000	8.45E-01	6.58E-01	3.51E+00	5.66E-01	1.78E+00
4000	3.90E-01	4.04E-01	2.20E+00	3.78E-01	
5000		2.64E-01	1.10E+00	1.37E-01	9.67E-01

Note: Unit for confining pressure and permeability are psi and md

It was observed that both types of fractures had permeability values between 0.1 md to 10 md. There was no clear trend showing which type of fracture was of higher permeability. Thus, it was concluded that these two types of fractures had the same baseline permeability value. At 5000 psi confining stress, the average permeability value for the saw-cut fracture was 6.82E-01 md and for the sheared fracture it was about 5.52E-01 md.

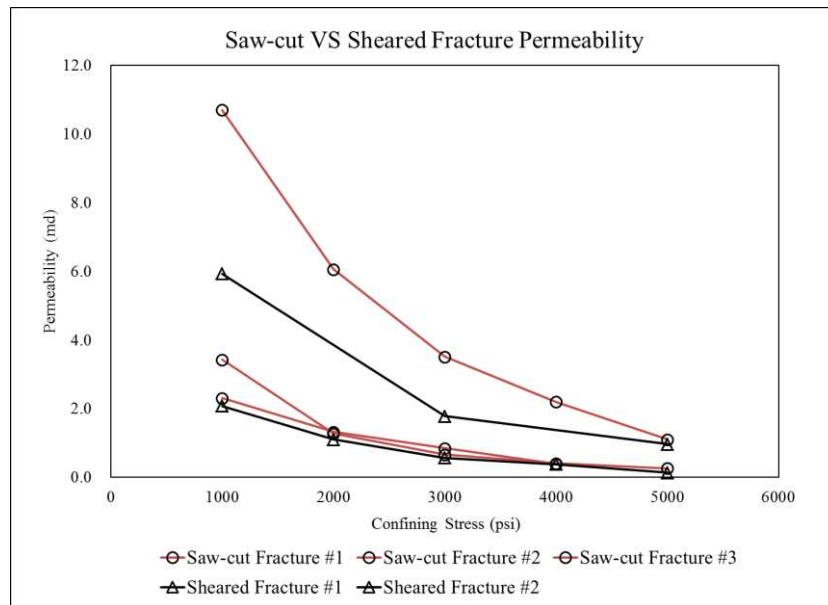


Figure 4.4 Saw-cut versus sheared fracture permeability.

In addition, as almost all of the fractures were used for more than two proppant tests, the embedment and the fatigue of the rock could have changed the baseline permeability value of these fractures; therefore, it was important to know if the change was big enough to affect the credibility of the test result. The permeability of the saw-cut fracture #3 in Figure 4.4 was tested

after three proppant tests. Including the baseline permeability test, this core was tested four times before retesting the fracture permeability. The comparison is shown in Figure 4.5.

Table 4.3 Fracture permeability before and after used.

Confining Pressure (psi)	Saw-cut Fracture #3 before proppant test (md)	Saw-cut Fracture #3 after proppant test (md)
1000	1.07E+01	9.30E+00
2000	6.06E+00	5.34E+00
3000	3.51E+00	3.34E+00
4000	2.20E+00	2.08E+00
5000	1.10E+00	9.83E-01

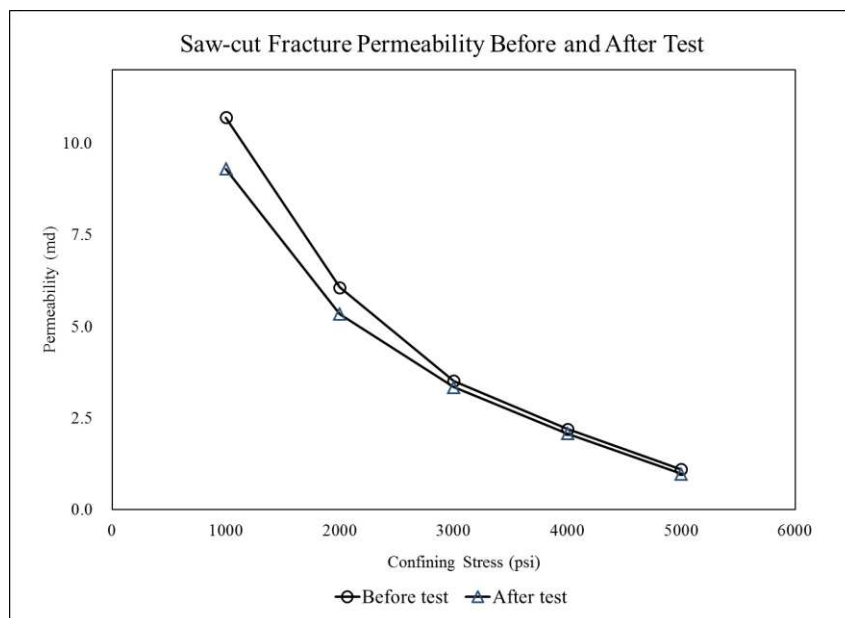


Figure 4.5 Saw-cut fracture permeability before and after proppant test.

It was observed that multiple uses of the shale rock fracture surface did not change the fracture baseline permeability by much. This comparison verified that the reuse of fracture surface is not a dominant factor in the proppant tests discussed later.

### 4.3 Proppant Test

In this section, for the convenience of reading and recognition, different colors are used to represent different proppant concentrations in each plot. The unit of proppant concentration

for all the data is lb/ft<sup>2</sup>. If not mentioned, the generic placement pattern for each concentration is a random pattern; clustered placement is mentioned separately. The relationship is shown in Table 4.4.

Table 4.4 Color and proppant concentration relationship.

Color	Proppant concentration (lb/ft <sup>2</sup> )
Black	0.03
Dark blue	0.02
Tan	0.015
Red	0.01
Orange	0.005
Purple	0.001
Light green	Clustered 0.01

The pictures of three conventional proppants before and after the test with proppant concentration of 0.005 lb/ft<sup>2</sup> are shown in Figure 4.6.

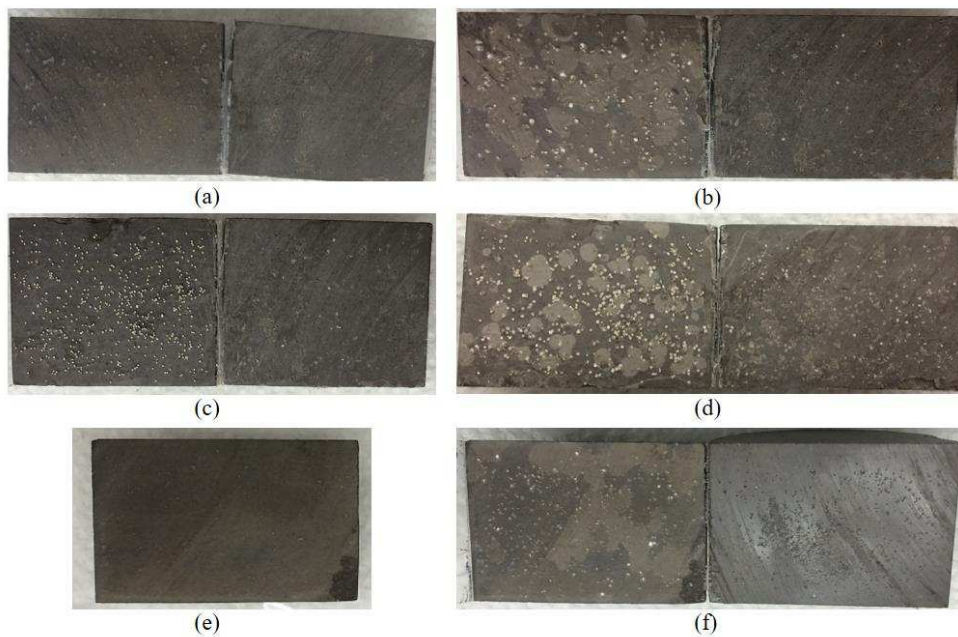


Figure 4.6 Conventional proppant before and after test at 0.005 lb/ft<sup>2</sup> concentration: (a) white sand 30/70 before test (b) white sand 30/70 after test (c) LWC 40/80 before test (d) LWC 40/80 after test (e) white sand 100 mesh before test (f) white sand 100 mesh after test.

It was observed that white sand 30/70 had wider mesh size range, and bigger size proppants were crushed first. The mesh size distribution for LWC 40/80 was more even. The

picture after the test shows that LWC were almost evenly supporting the fracture surface. White sand 100 mesh had more proppant number on the fracture surface.

#### **4.3.1 Lightweight Ceramic (LWC) 40/80**

Five different tests were done with LWC proppant within saw-cut fractures. The test results are shown in Table 4.5. The decline pattern of permeability versus confining stress is shown in Figure 4.7. Each color represents a proppant concentration. It was observed that initially, when confining stress was low, every proppant concentration had high permeability value at around  $1.0E4$  to  $1.0E5$  md. With increasing confining stress, the permeability values start to decrease. At the end, when confining stress reaches 5000 psi, the permeability values of different proppant types vary from around 10 md to  $1.0E04$  md. In addition, the decline pattern (slope) of each proppant concentration is also different.

Figure 4.8 includes the plot of the permeability value versus proppant concentration with different confining stresses. Note that the critical monolayer concentration for this type of proppant is around  $0.07$  lb/ft<sup>2</sup>. The maximum proppant concentration tested in this research is around  $0.02$  lb/ft<sup>2</sup>; it is below one third of the critical monolayer concentration.

It is observed in all the tests that when proppant concentration is low and confining stress is low, the permeability value is always higher than the permeability value of proppant pack with higher proppant concentration. The reasons could be: 1) small confining stress is still not high enough to crush the proppant pack; 2) the proppants on the fracture surface acts like pillars in clustered proppant fracturing technique. The infinite conductivity flow path between the pillars decrease with increasing amount of proppants on the fracture surface, as a result permeability decreased.

Table 4.5 Permeability test result for LWC 40/80.

Confining Pressure	LWC40/80#1 0.02 Conc.	LWC40/80 #2 0.01 Conc.	LWC40/80#3 0.005 Conc.	LWC40/80#4 0.001 Conc.	LWC40/80#5 Clustered 0.01 Conc.
1000	3.63E+04	1.82E+04	2.69E+04	1.11E+04	4.72E+04
2000	2.30E+04	1.65E+04	4.05E+03	1.57E+03	2.22E+04
3000	1.73E+04	1.24E+04	1.12E+03	1.76E+02	1.48E+04
4000	1.40E+04	6.55E+03	4.66E+02	2.82E+01	9.99E+03
5000	9.25E+03	1.85E+03	2.38E+02	7.06E+00	7.03E+03

Note: Units for confining pressure and permeability are psi and md

However, when confining stress increased, proppant pack permeability with really low concentration decreased quickly, especially the proppant pack with concentration around 0.001 lb/ft<sup>2</sup>. For proppant pack with concentration above 0.01 lb/ft<sup>2</sup>, the proppant pack tended to have higher stress resistance. It was also observed that a clustered proppant pack with a concentration around 0.01 lb/ft<sup>2</sup> performed close to a proppant pack with 0.02 lb/ft<sup>2</sup> concentration.

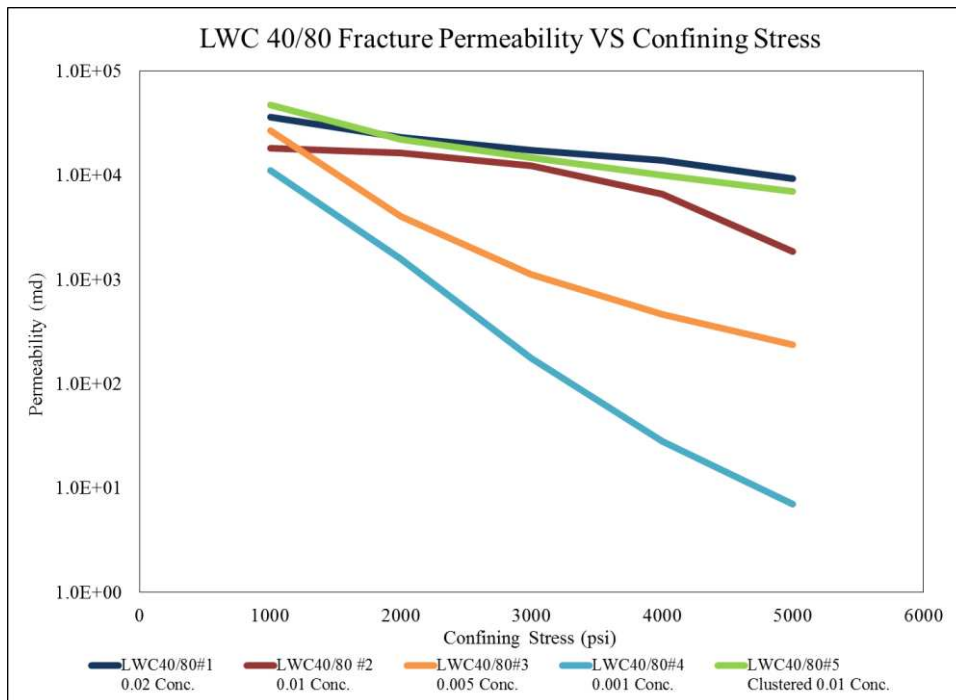


Figure 4.7 LWC 40/80 propped fracture permeability versus confining stress.

Figure 4.8 shows the trend of permeability versus concentration with different confining stresses. It was observed that for low confining stress, there was some variation of

permeability value. With higher confining stress, the permeability only increased with increasing proppant concentration. Brannon et al. (2004) discussed the optimal concentration value for Brady sand, which is around 0.6 lb/ft<sup>2</sup>. The optimal concentration for LWC 40/80 has not yet been discussed. From Figure 4.8 it seems the optimal concentration is above, yet closes, to 0.02 lb/ft<sup>2</sup>.

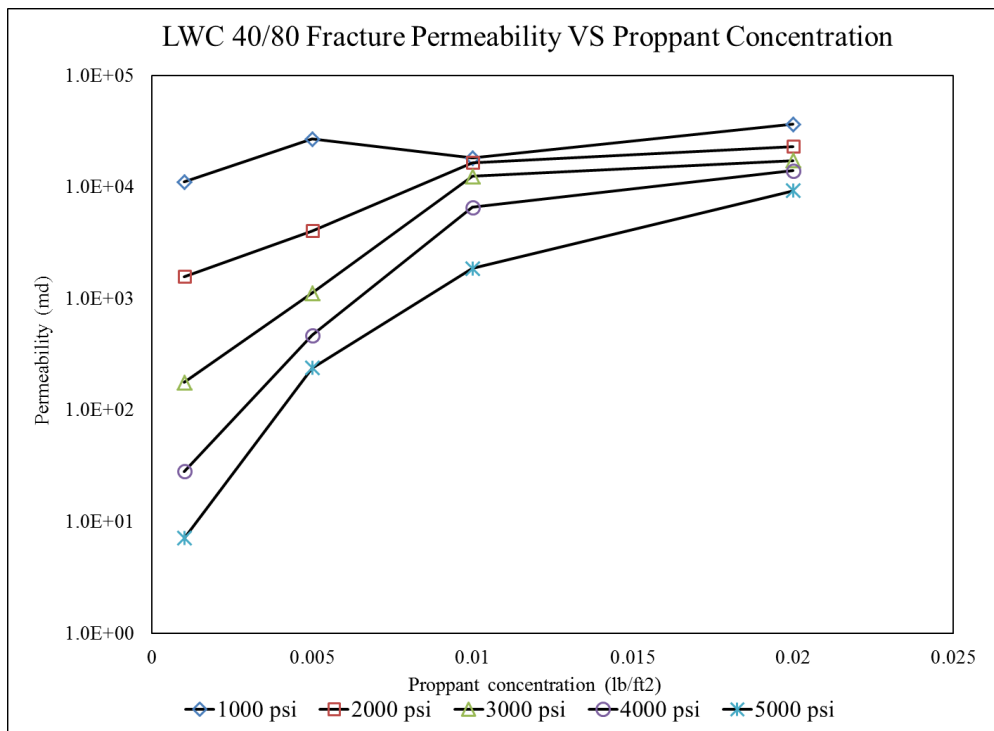


Figure 4.8 LWC 40/80 fracture permeability versus proppant concentration.

### 4.3.2 White Sand 30/70

Five different tests were done with white sand 30/70 proppant with saw-cut fractures. The test results are shown in Table 4.6. Note that the critical monolayer concentration for this type of proppant was around 0.085 lb/ft<sup>2</sup>. The maximum proppant concentration tested in this research was around 0.02 lb/ft<sup>2</sup>, which is about one fourth of the critical monolayer concentration.

Table 4.6 Permeability test result for white sand 30/70.

Confining Pressure	White Sand30/70 #1 0.02 Conc.	White Sand30/70 #1 0.01 Conc.	White Sand30/70#3 0.005 Conc.	White Sand30/70#4 0.001 Conc.	White Sand30/70 #5 Clustered 0.01 Conc.
1000	2.83E+04	4.07E+04	1.62E+04	1.01E+03	3.18E+04
2000	2.09E+04	2.60E+04	8.97E+03	2.63E+02	2.28E+04
3000	1.58E+04	1.95E+04	5.20E+03	5.51E+01	1.62E+04
4000	1.28E+04	1.21E+04	3.67E+03	1.66E+01	1.09E+04
5000	1.09E+04	8.52E+03	1.20E+03	7.50E+00	8.17E+03

Note: Unit for confining pressure and permeability are psi and md

The decline pattern of permeability versus confining stress is shown in Figure 4.9, similar to LWC 40/80, when confining stress was low, a high permeability value could be obtained. However, only proppant concentrations above 0.01 lb/ft<sup>2</sup> showed higher stress resistance.

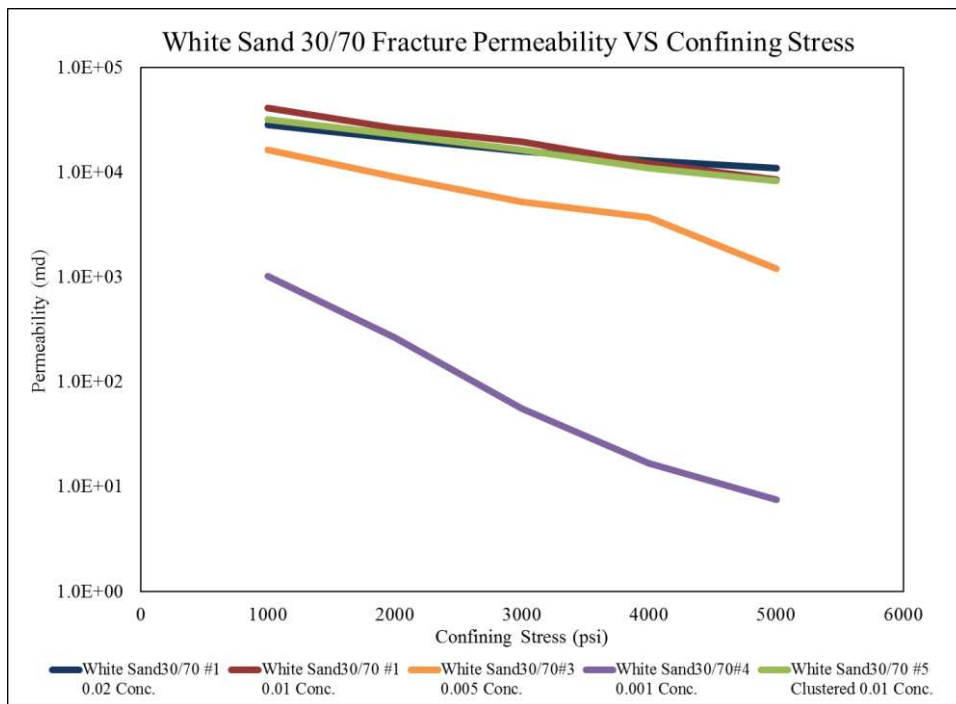


Figure 4.9 White sand 30/70 fracture permeability versus confining stress.

Figure 4.9 shows the trend of permeability versus concentration with different confining stresses. For confining stresses from 1000 psi to 3000 psi, 0.01 lb/ft<sup>2</sup> is an optimal value for fracture permeability. However, with increasing confining stress, the highest permeability is obtained only by the highest proppant concentration 0.02 lb/ft<sup>2</sup>. This is similar to the trend observed in LWC 40/80. Again, a clustered proppant pack is of high permeability and stress resistance even with lower absolute concentration value.

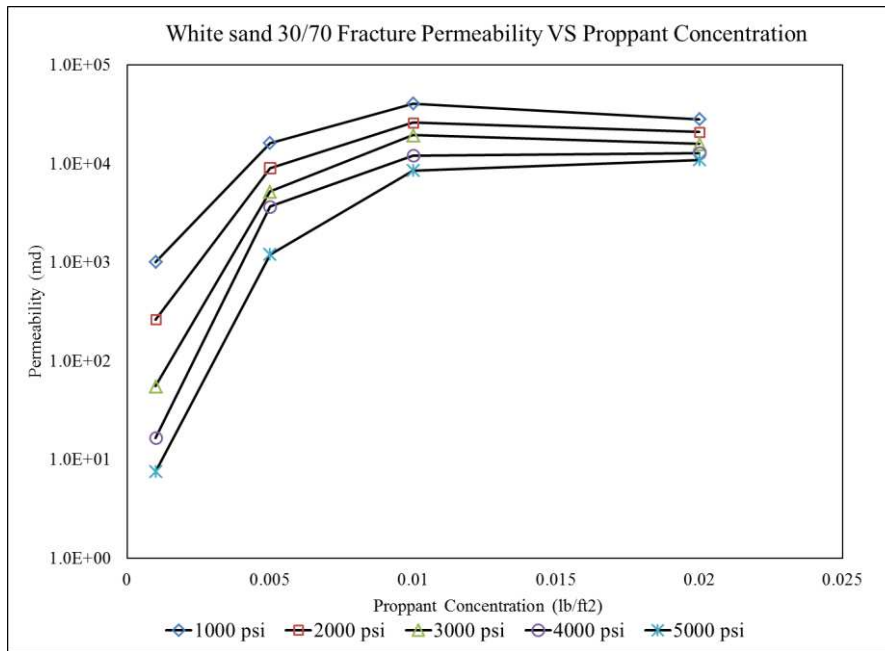


Figure 4.10 White sand 30/70 fracture permeability versus proppant concentration.

### 4.3.3 White Sand 100 Mesh

Five different tests were done with white sand 100 mesh proppant with saw-cut fractures. The test results are shown in Table 4.7. Note that the critical monolayer concentration for this type of proppant was around 0.043 lb/ft<sup>2</sup>. The maximum proppant concentration tested was around 0.02 lb/ft<sup>2</sup>, which is about one half of the critical monolayer concentration.

Table 4.7 Permeability test result for white sand 100 mesh

Confining Pressure	White Sand100#1 0.02 Conc.	White Sand100#3 0.01 Conc.	White Sand100#4 0.005 Conc.	White Sand100#5 0.001 Conc.	White Sand 100#6 Clustered 0.01 Conc.
1000	1.38E+03	2.63E+03	1.22E+03	1.93E+02	3.07E+04
2000	1.32E+03	1.82E+03	3.86E+02	9.14E+01	1.77E+04
3000	1.04E+03	9.71E+02	1.55E+02	4.78E+01	1.09E+04
4000	7.80E+02	6.09E+02	5.72E+01	2.16E+01	6.60E+03
5000	5.69E+02	2.92E+02	2.60E+01	8.84E+00	4.28E+03

Note: Unit for confining pressure and permeability are psi and md

The decline pattern of permeability versus confining stress is shown in Figure 4.11. All of the points decline quite linearly in this semi-log plot. Still, 0.02 lb/ft<sup>2</sup> holds the highest stress resistance within the random placement pattern group. Clustered proppant with 0.01 lb/ft<sup>2</sup> had the highest permeability performance among all types of proppant.

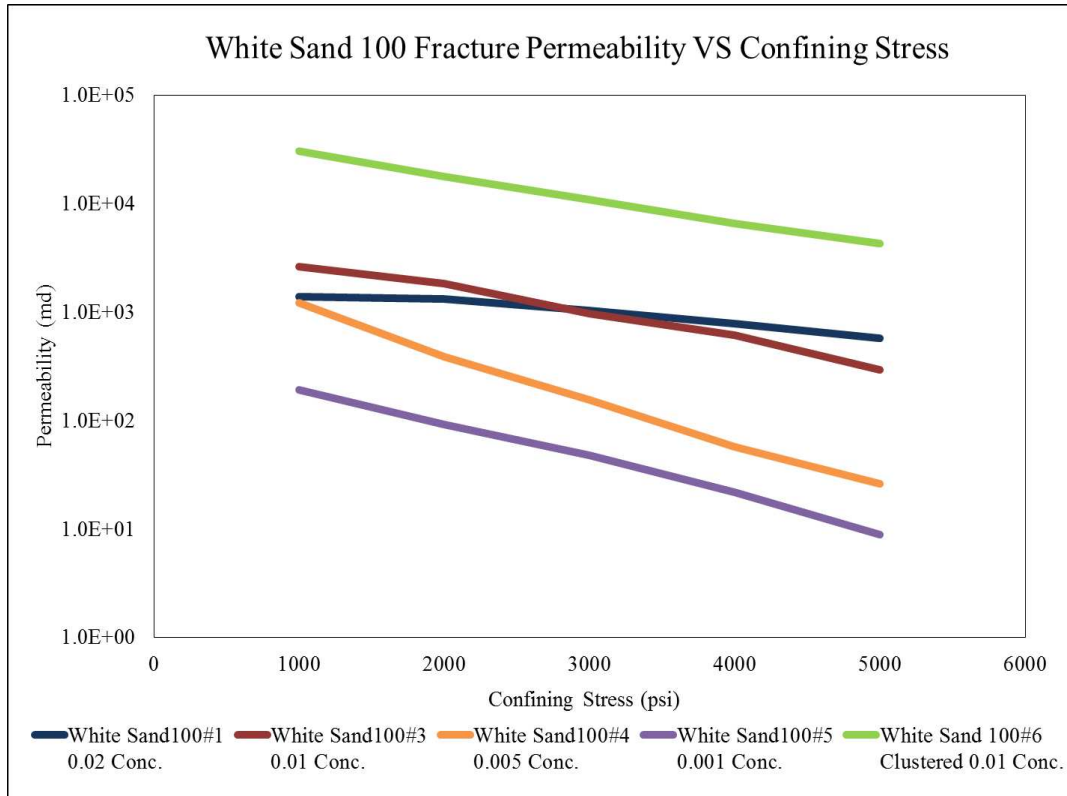


Figure 4.11 White sand 100 mesh fracture permeability versus confining stress.

Figure 4.12 shows the trend of permeability versus concentration with different confining stresses for white sand 100 mesh. From 1000 psi to 4000 psi, 0.01 lb/ft<sup>2</sup> is the optimal concentration value in regard to permeability value. However, at 5000 psi permeability, 0.02 lb/ft<sup>2</sup> proppant pack shows the highest permeability. It is possible that at higher confining pressure, more proppant is required to hold the fracture. When proppant concentration is low, the stress resistance of proppant pack is low, even if it has the advantage to form a “Pillar-like” pack that shows relatively high conductivity.

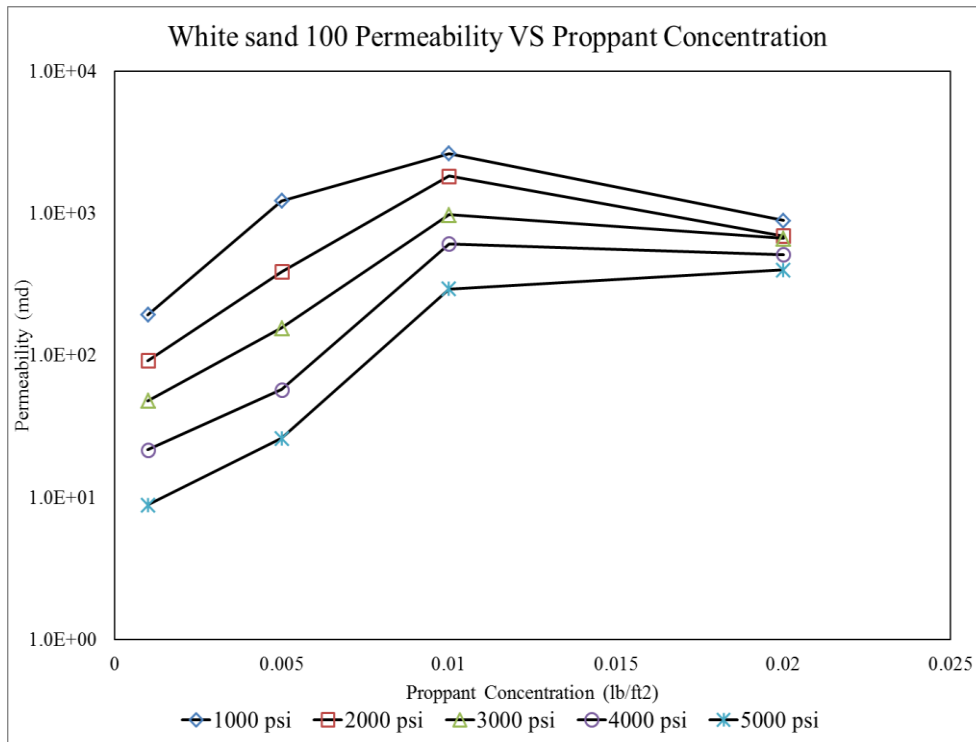


Figure 4.12 White sand 100 mesh permeability versus proppant concentration.

### Comparison at 5000 psi confining stress

The trend of permeability versus concentration at 5000 psi for these three types of proppant is plotted in Figure 4.13. The maximum permeability value for LWC 40/80 and white sand 30/70 are both close to  $1.0E4$  md. The average diameter of white sand 30/70 is higher; this could be the reason why at lower concentrations white sand 30/70 has higher permeability value. Yet, the permeability value of LWC 40/80 keeps increasing while white sand 30/70 tends to stabilize. The trend of white sand 30/70 and white sand 100 mesh is similar in shape yet different in absolute value.

All three types of proppant have permeability around  $8E1.0$  md with  $0.001$   $lb/ft^2$  proppant concentration. From lab observation it is about a dozens of proppant on the fracture surface if fracture dimension is  $1$  inch $\times$  $1$  inch and proppant type is 40/80. This value is still more than ten times larger than the average  $6.82E-1.0$  md for saw-cut fracture.

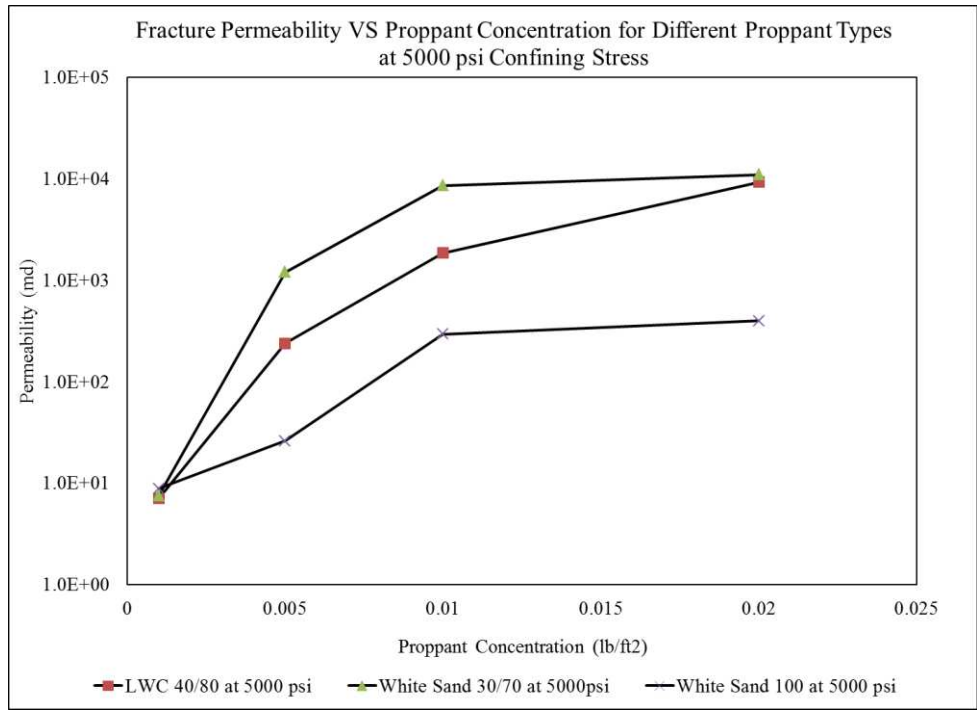


Figure 4.13 Fracture permeability versus proppant concentration for different proppant types at 5000 psi confining stress.

#### 4.3.4 ULW 30/80

ULW proppant was tested in two types of fractures: saw-cut fracture and sheared fracture. In saw cut fractures, three concentrations were tested: 0.01 lb/ft<sup>2</sup>, 0.02 lb/ft<sup>2</sup> and 0.03 lb/ft<sup>2</sup>. In sheared fractures, refined steps from 0.001 lb/ft<sup>2</sup> to 0.02 lb/ft<sup>2</sup> were tested. Different decline patterns were observed when comparing with the three conventional proppant types. Note that for ULW 30/80, its critical monolayer proppant concentration was around 0.03 lb/ft<sup>2</sup>.

##### *ULW30/80 in saw-cut fracture*

Two tests were done for concentrations equaling 0.02 lb/ft<sup>2</sup>. The permeability versus confining stress with different concentrations are listed in Table 4.8 and plotted in Figure 4.14.

Table 4.8 Permeability test result for ULW 30/80 in saw-cut fractures.

Confining Pressure	ULW30/80#1 0.03 Conc.	ULW30/80#2 0.02 Conc.	ULW30/80#3 0.02 Conc.	ULW30/80#5 0.01 Conc.	ULW30/80#6 Clustered 0.01 Conc.
1000	4.35E+03	7.10E+03	6.42E+03	1.76E+04	7.39E+04
2000	3.50E+03	5.70E+03	5.80E+03	1.40E+04	5.90E+04
3000	1.60E+03	4.86E+03	4.57E+03	9.43E+03	4.29E+04
4000	8.85E+02	2.89E+03	2.23E+03	7.59E+03	3.95E+04
5000	4.09E+02	1140	1.06E+03	5.97E+03	2.77E+04

Note: Unit for confining pressure and permeability are psi and md

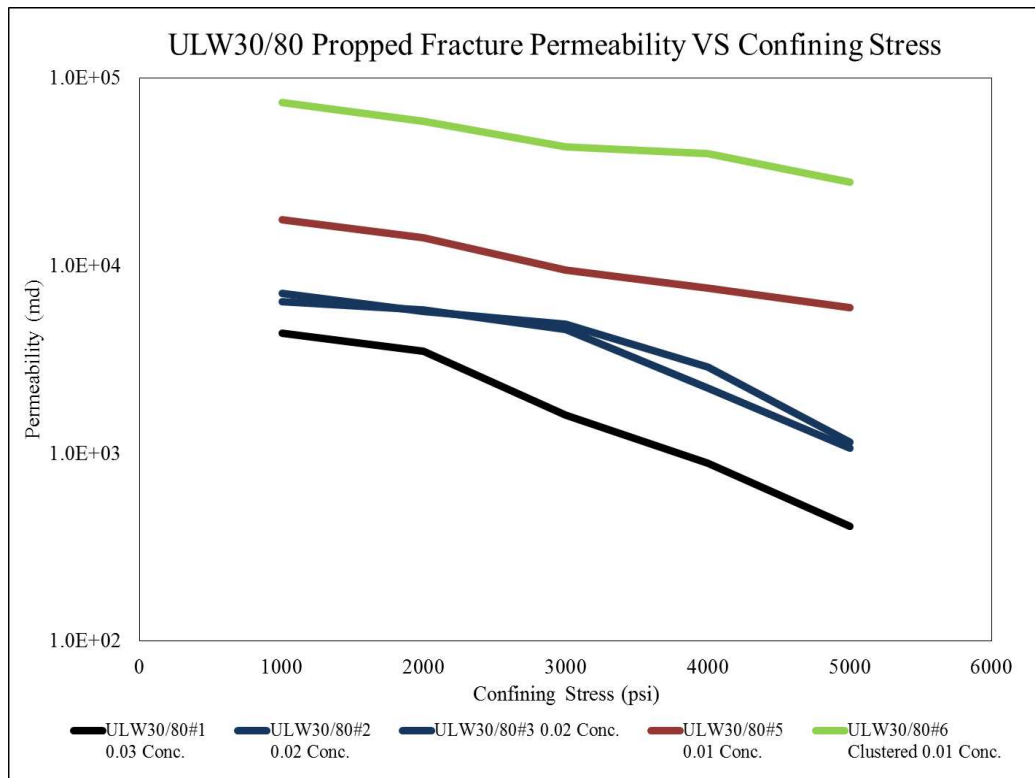


Figure 4.14 ULW 30/80 propped saw-cut fracture permeability versus confining stress.

Different from all the other types of conventional proppants, the permeability value of ULW 30/80 decreased with increasing proppant concentration. This trend is also seen in Figure 4.15. As the saw-cut fracture permeability was tested already, it is logical to speculate that from zero proppant concentration to 0.03 lb/ft<sup>2</sup> proppant concentration permeability, there should be an increase first and then a decrease. This phenomenon is observed in the tests done in sheared fractures. However, similar to what was observed with conventional proppants, the clustered

proppant pack still showed better permeability performance with 0.01 lb/ft<sup>2</sup> proppant concentration.

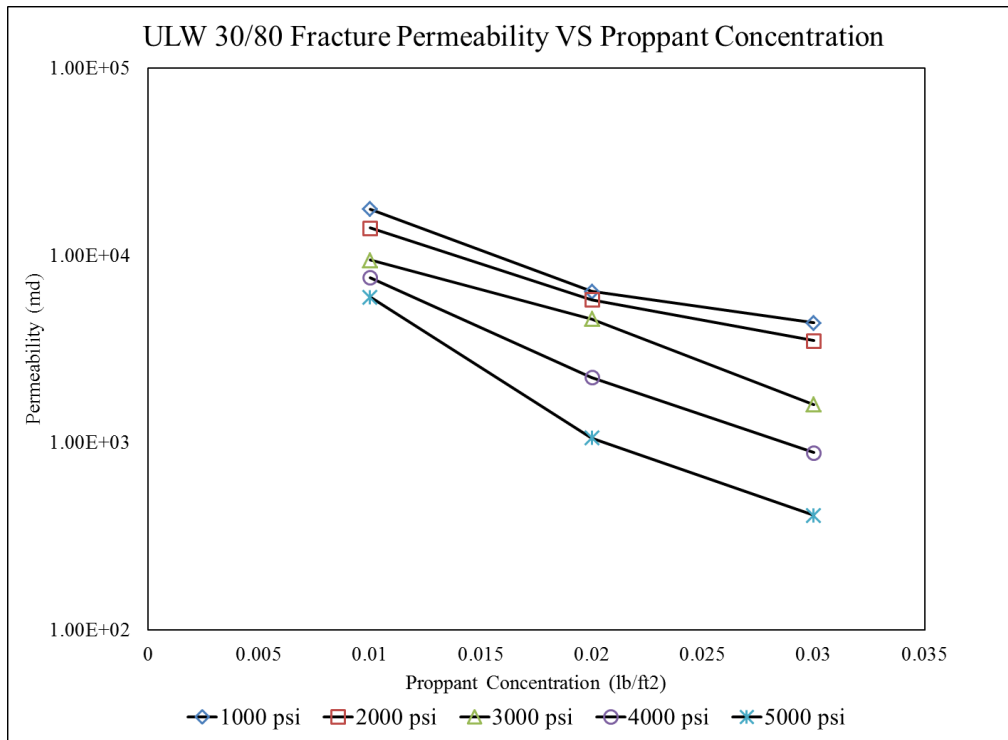


Figure 4.15 ULW 30/80 propped saw-cut fracture permeability versus proppant concentration.

***ULW30/80 in sheared fracture***

Refined concentration stages were tested in sheared fractures for ULW 30/80. It was expected that the surface roughness of the sheared fractures would reflect the real proppant performance in the real world.

Table 4.9 Permeability test result of ULW 30/80 in sheared fractures

Confining Pressure	ULW30/80 #1 0.02 Conc.	ULW30/80 #2 0.015 Conc.	ULW30/80 #3 0.01 Conc.	ULW30/80 #4 0.005 Conc.	ULW30/80 #5 0.001 Conc.
1000	8.24E+03	5.38E+03	7.16E+03	1.95E+03	2.17E+01
2000	3.04E+03	2.47E+03	3.01E+03	4.17E+02	9.97E+00
3000	1.00E+03	1.24E+03	1.34E+03	2.56E+02	5.98E+00
4000	4.76E+02	4.52E+02	9.25E+02	1.79E+02	3.72E+00
5000	2.88E+02	3.11E+02	6.61E+02	1.08E+02	2.13E+00

Note: Unit for confining pressure and permeability are psi and md

The decline pattern of permeability versus confining stress is shown in Figure 4.16. As expected, permeability performance improved from 0.001 lb/ft<sup>2</sup> to 0.01 lb/ft<sup>2</sup>, yet decreased after 0.01 lb/ft<sup>2</sup>.

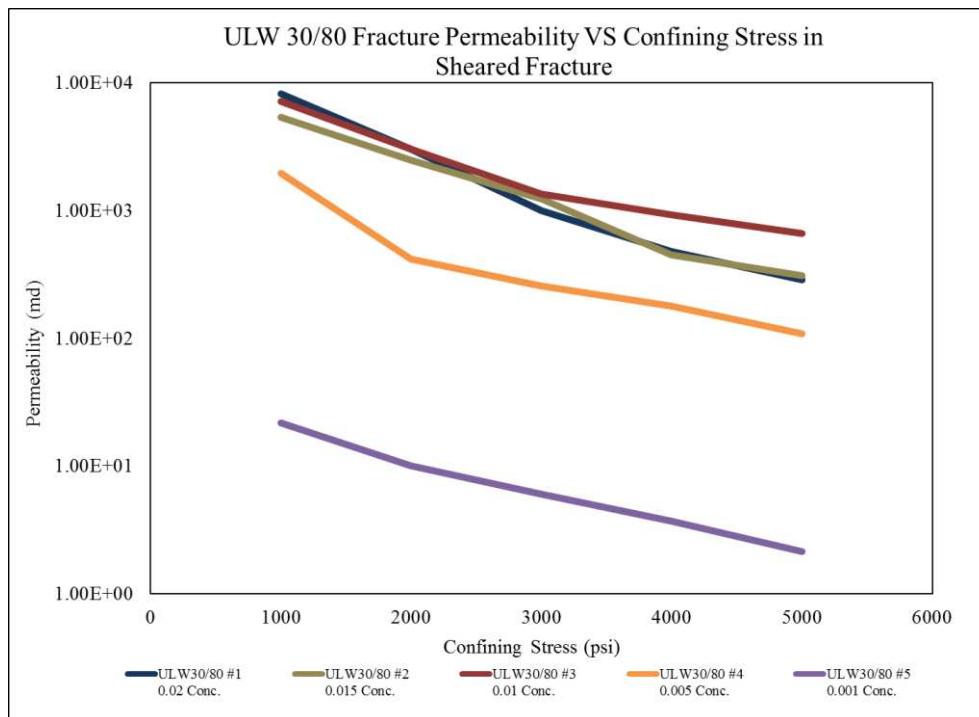


Figure 4.16 ULW 30/80 Fracture permeability versus confining stress in sheared fracture.

Figure 4.17 shows the trend of permeability versus concentration with different confining stresses for ULW 30/80 in sheared fractures. Contrary to any type of conventional proppant, ULW clearly showed an optimal concentration value around 0.01 lb/ft<sup>2</sup>, especially when confining stress was high. The reason could be the fact that ULW has a relatively higher plasticity property. Its documented Young's Modulus is around 25000 psi. This value is significantly less than general shale and conventional proppants. Thus, this proppant deforms largely with increasing confining stress. However, it is also documented that this kind of product tends to stay intact after it has been squeezed to a certain point.

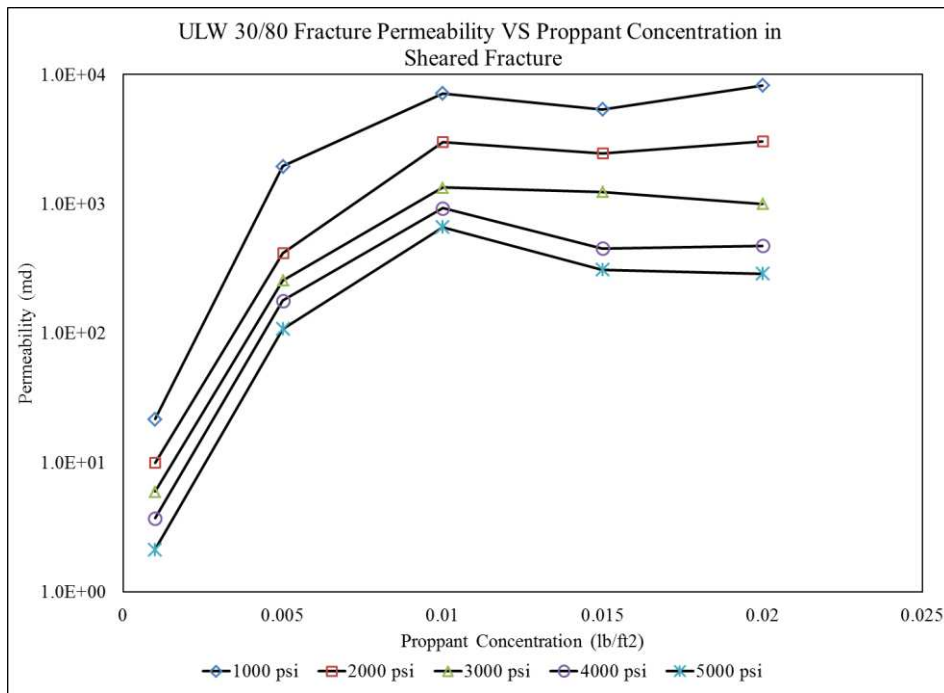


Figure 4.17 ULW 30/80 fracture permeability versus proppant concentration in sheared fractures.

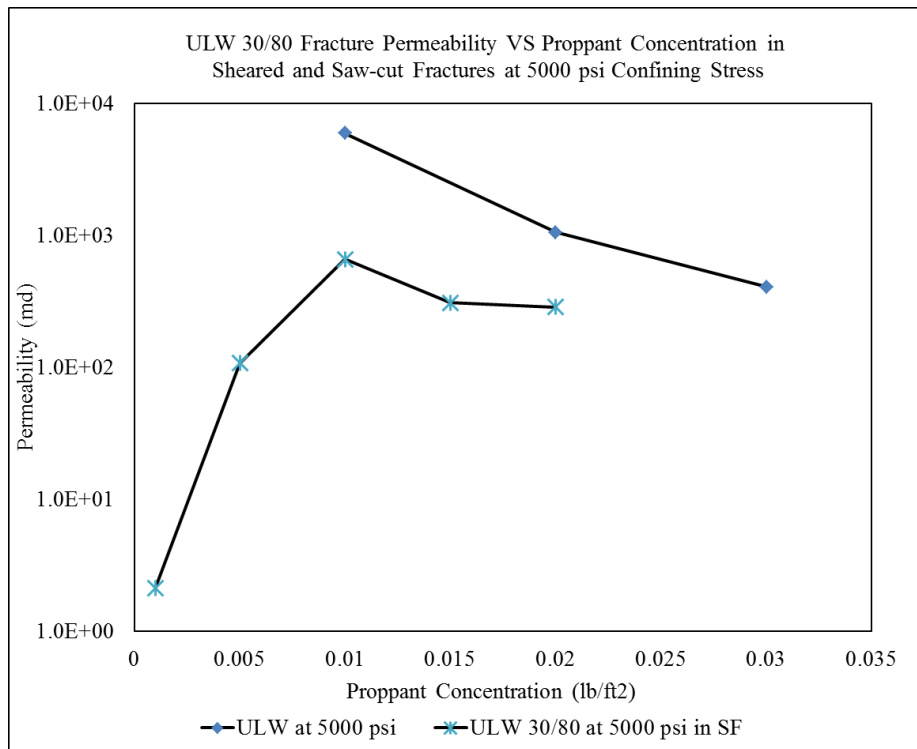


Figure 4.18 ULW 30/80 fracture permeability versus proppant concentration in both sheared and saw-cut fracture at 5000 psi confining stress.

The permeability tested for ULW 30/80 versus concentration in saw-cut fracture and sheared fracture is compared in Figure 4.18. From 0.01 lb/ft<sup>2</sup> to 0.02 lb/ft<sup>2</sup>, the decline of permeability tested in these two kinds of fractures was the same, yet the absolute value was different. The possible reasons could be the effect of fracture roughness; this is discussed in detail in later section.

#### **4.4 Detailed Discussion**

This section discusses the trends that were discovered in the experiments. This discussion will lead to the final conclusions of this research.

##### **4.4.1 Experiment Limitations**

The limitations that were encountered in this research must be mentioned first. These are

- The random placement of proppant on the fracture. The placement was only conducted by hand; thus, it was not always perfectly random.
- The maximum confining stress. Five thousand psi was used because the outcrop shale samples might have failed above this value. Failure of rock can cause immense damage to CMS-300, and thus it was avoided.
- Fracture width. To calculate conductivity, the fracture width is needed, yet this can hardly be observed with tests in CMS-300. Considering the fact that when proppant concentration is below monolayer no packing process is involved, the variation of fracture width should be small.
- Damage mechanism. Only stress sensitivity was analyzed in this research, no other damage mechanisms were considered.

- Flowing fluid in test. CMS-300 uses the pressure transmission method to calculate permeability. The fluid (usually helium) flows through the fracture in an unsteady state; this is difficult to compare with steady state tests done with conductivity cell.
- The permeability measured in this research followed the requirement of CMS-300 test procedure exactly. The input dimensions were measured to describe the whole core instead of the fracture. Thus, the measured permeability is actually close to the effective permeability of a core with a propped fracture in it. In API or ISO 13505 proppant tests, the dimensions are purely about the fracture itself. In addition, the testing condition is not in steady state comparing with conductivity cell test. Thus, it is not expected that the permeability values obtained in this research is comparable with lab conductivity test results.

#### **4.4.2 Conventional Proppant in SRV**

Three types of conventional proppants were tested: LWC 40/80, white sand 30/70 and white sand 100 mesh. These kinds of proppants are popularly used in hydraulic fracturing operations in shale plays. The purpose was to analyze their contribution to the fracture conductivity distribution in the SRV system, especially around the tip of fractures where it is logical to assume that fractures are not well propped by these proppants.

#### ***Permeability architecture in SRV***

The critical monolayer concentration for LWC 40/80, white sand 30/70 and white sand 100 mesh are 0.069 lb/ft<sup>2</sup>, 0.084 lb/ft<sup>2</sup> and 0.043 lb/ft<sup>2</sup>. Before any comparison is made, the ratio between the tested concentration and its critical monolayer concentration must be listed.

Table 4.10 Ratio of tested concentration to critical monolayer concentration for different proppant types.

Proppant type	Proppant concentration				
	0.001	0.005	0.01	0.02	0.03
<b>ULW 30/80</b>	3.24%	16.20%	32.40%	64.80%	97.20%
<b>LWC 40/80</b>	1.44%	7.20%	14.41%	28.82%	43.22%
<b>White Sand 30/70</b>	1.18%	5.92%	11.84%	23.68%	35.52%
<b>White Sand 100</b>	2.35%	11.74%	23.48%	46.96%	70.44%

From Figure 4.13, it is observed that at 5000 psi confining, these conventional proppants with only 0.001 lb/ft<sup>2</sup> concentration have permeability around 7.5 md. The average saw-cut fracture permeability at 5000 psi is around 0.68 md. The propped fracture permeability is more than ten times the unpropped fracture permeability. At the same time, the naturally fractured shale sample has permeability around 1.56E-03 md; the permeability architecture is observed here.

***Optimal proppant type for SRV***

Figure 4.13 shows proppant performance at 5000 psi confining stress. First, between white sand 30/70 and white sand 100 mesh, although white sand 30/70 has higher permeability when proppant concentration is high, with the decrease of proppant concentration, they reached the same permeability value. If the data in Table 4.10 is considered, when proppant concentration is 0.001 lb/ft<sup>2</sup>, white sand 100 mesh actually has more proppant on the fracture surface. Compare the difference between white sand 30/70 and LWC 40/80, when concentration is between 0.001 lb/ft<sup>2</sup> and 0.02 lb/ft<sup>2</sup>, white sand 30/70 shows better permeability performance. This could due to its larger average proppant size. However, the trend shows that with an increase in proppant concentration, LWC 40/80 will surpass white sand 30/70. Higher proppant strength and more even mesh distribution of LWC 40/80 could be the reason for this trend.

The proppant transportation process should also be considered. Although white sand 30/70

has better permeability performance at low concentrations, the fracturing fluid in the real world might be unable to transport proppant to the tips of fractures, especially in a low viscous slickwater system. Proppant transportation tests has already shown that larger proppants tend to settle first, following Stoke's law.

#### **4.4.3 ULW Proppant in SRV**

Lab proppant transportation has already shown that ULW has potential to occupy the higher side of an opened fracture, and the placement pattern could possibly be partial monolayer; thus, it is meaningful to test the permeability of ULW with concentrations below monolayer. Note that most of the tests for ULW 30/80 were done in sheared fracture.

##### ***Optimal value for ULW 30/80***

Similar to conventional proppant, ULW 30/80 has high permeability performance with really low proppant concentrations. The 0.001 lb/ft<sup>2</sup> ULW 30/80 tested has permeability around 2.13 md. This is still about four times the average sheared fracture permeability.

The difference between ULW 30/80 and conventional proppants has been documented in other papers, what is observed in this research is that ULW 30/80 clearly shows an optimal concentration around 0.01 lb/ft<sup>2</sup>. The reason could be that the ULW proppant is lighter than conventional proppant, and thus it has more proppant numbers at the same proppant concentration. When the proppant concentration increases, as ULW proppant material is highly deformable, the porosity of proppant pack decreases. This may cause the fracture to lose much of its permeability.

A good aspect of this product is that it stays intact even if it is highly deformed, which

makes it a good material at low proppant concentrations, especially when considering its accessibility to the higher side of a fracture. With the permeability tested in this research, if a lab transportation test could verify the exact proppant concentration range that will be formed by ULW proppant, then the contribution of ULW proppant in the real world can be accurately analyzed.

### ***Embedment effect***

Another good aspect of ULW proppant is that this proppant does not have embedment effect. See Figure 4.19.

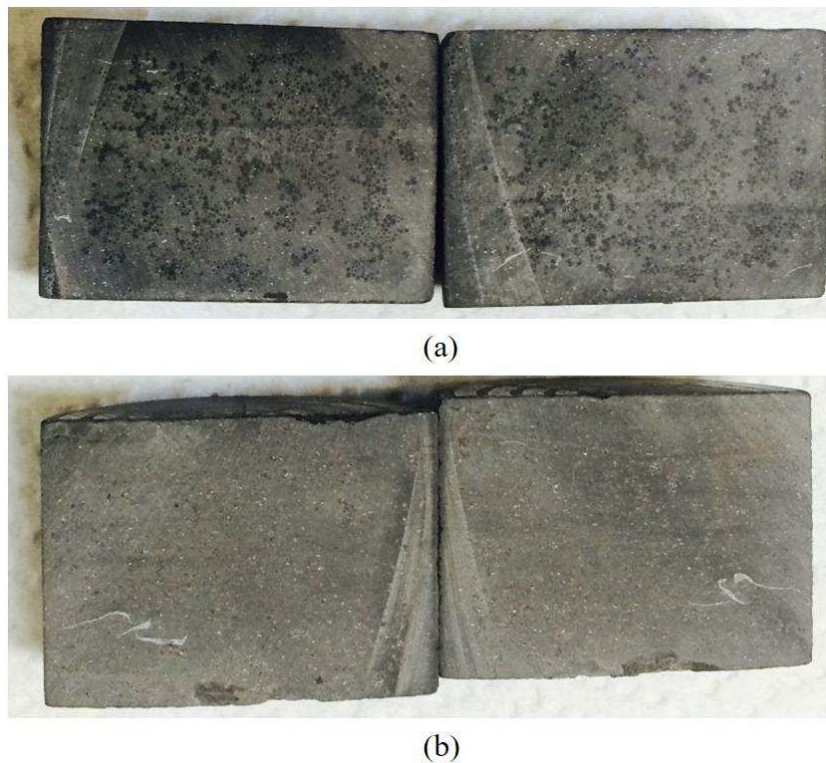


Figure 4.19 Embedment effect for fractures with ULW 30/80 and white sand 100 mesh; (a) ULW 30/80 shows no embedment effect; (b) white sand 100 mesh shows embedment effect.

ULW proppant shows nominal embedment: only dark marks on the fracture surface, while white sand 100 mesh propped fracture after test has clear embedment effect on the fracture surface. This embedment effect is also observed in LWC 40/80 and white sand 30/70.

The observation that ULW proppant has negligible embedment effect is only happened in this research when only stress effect is considered. It only tells that the natural “weaker” property of ULW proppant makes its physical interaction with rock surface not as strong as conventional proppant. To quantify either this kind of proppant has embedment effect or not, or how much embedment effect it should have in real world, more tests considering various damage mechanisms should be conducted. For example, it is documented that liquid (chemical) and temperature will affect the rock mechanics of Niobrara shale dramatically (Corapcioglu et al. 2014).

#### ***ULW in sheared fracture***

Proppant permeability declines faster in sheared fractures compared with saw-cut fractures. This could be due to the rough surface geometry of sheared fractures. See Figure 4.20. In lower concentration proppant all crushed during test. Yet in higher concentrations, only a part of proppants was crushed. The proppant lies in the grooves not only do not support the fracture, but also could block the flow path. This fracture roughness effect could happen in all kinds of proppants and change their permeability decline curve. This effect is usually ignored in multilayer proppant tests as the overall proppant pack width is much wider than the fracture aperture. However, in proppant low concentration test, or test for products like ULW proppant that might naturally form partial monolayer proppant pack in fractures, this effect should be considered as a damage factor to the measured fracture permeability. Form the observations of this research, permeability decline pattern will deviate at a large scale if fracture with surface roughness is used.



(a)



(b)



(c)

Figure 4.20 Fracture roughness effect: (a) 0.001 lb/ft<sup>2</sup> ULW 30/80 proppant, all been crushed; (b) 0.01 lb/ft<sup>2</sup> ULW 30/80 proppant, all been compressed; (c) 0.02 lb/ft<sup>2</sup> ULW 30/80 proppant, some been crushed, some been compressed, a lot stay new after test.

#### 4.4.4 Cluster Proppant Pack

It was observed in almost all the tests that cluster proppant pack could have higher permeability and stress resistance even with a smaller proppant concentration. In all of the tests clustered 0.01 lb/ft<sup>2</sup> either performs better or close to the 0.02 lb/ft<sup>2</sup> with the same proppant type. This reveals the potential for clustered hydraulic fracturing techniques. However, in the study of clustered proppant, the placement pattern is still not sure. The placement pattern used in this research might not reflect the situation in the real world. This leads to the numerical modeling of clustered proppant fracturing in the next chapter.

## CHAPTER 5

### NUMERICAL MODELING OF CLUSTERED PROPPANT

To account for the uncertainty of the placement pattern of different types of clustered proppant fracturing, a simple model was built using COMSOL Multiphysics.

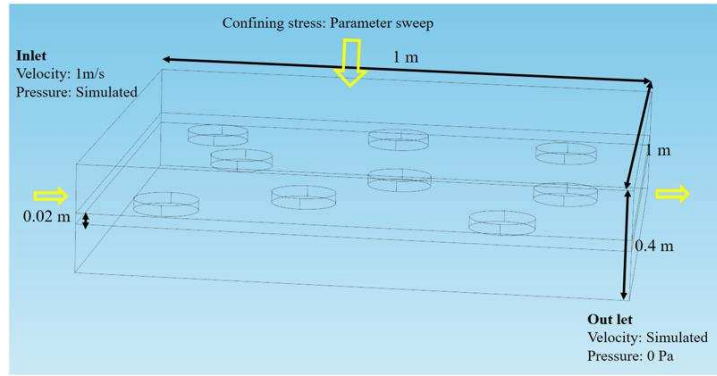
#### 5.1 Model Setup

The geometry of the model is shown in Figure 5.1. The overall shape is a  $1\text{m}\times 1\text{m}\times 0.4\text{m}$  block. In the middle, nine pillars are sandwiched in a fracture with width of 0.02 m. The diameter of the pillar is 0.06 m. The plates and the pillars were assigned different solid mechanics properties in the model for sensitivity analysis. Confining stress is from the top to simulate the piston force in conductivity cells.

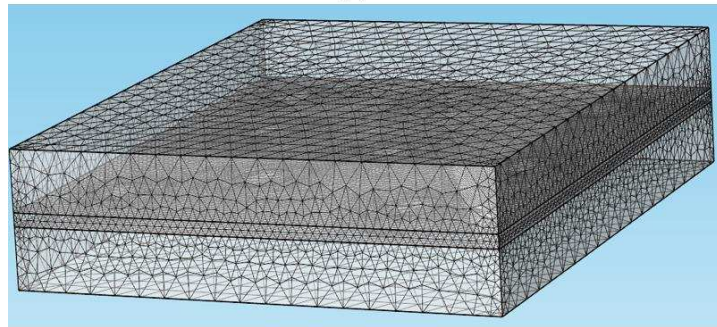
“Laminar Flow” physics is also included apart from the “Solid Mechanics” part. The domains of “Laminar Flow” and “Solid Mechanics” are shown in Figure 5.2. An “Arbitrary Lagrangian-Eulerian (ALE)” type of “Moving Mesh” was used so that the “Laminar Flow” domain could capture the deformation of flow field due to the effect of confining stress. “Parameter Sweep” was used to test multiple stress values in the same run.

#### 5.2 Simulation Example

Random placement and ordered placement patterns are considered in this example. In random placement, the proppants are randomly placed on the fracture surface. In ordered placement, the proppants are arranged in an array. Here these two types of placement patterns are not assumed to be true real world, they were simply used to check if the model built is sensitive to different types of placement patterns.

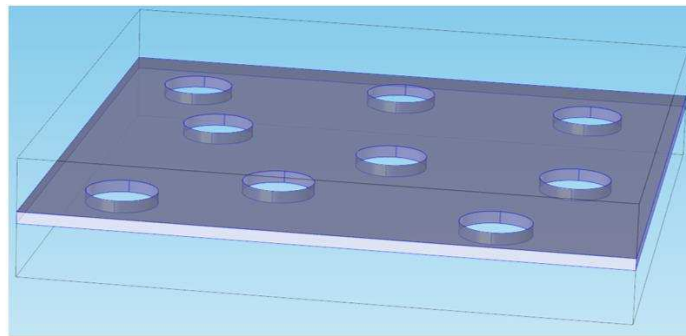


(a)

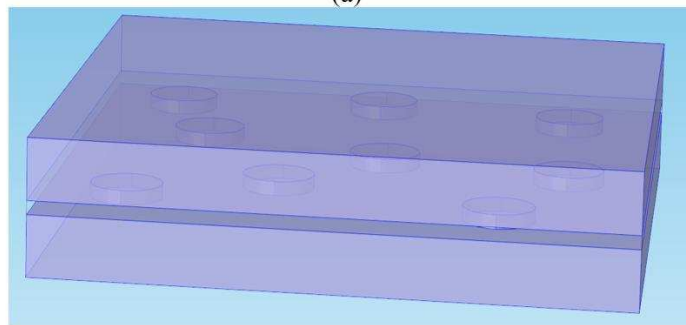


(b)

Figure 5.1 Model setup for clustered proppant simulation: (a) geometry model and basic physics setup for modeling; (b) physics controlled mesh setup for modeling.



(a)



(b)

Figure 5.2 Domain of flow field and solid mechanics: (a) flow field for “Laminar flow”; (b) solid mechanics domain.

“Solid Mechanics” requires Young’s modulus, Poisson’s ratio, and density as necessary inputs. As proppant products usually are not provided with Young’s modulus and Poisson’s ratio, they are assumed in this model. The assigned input “Solid Mechanics” values are shown in Table 5-1.

Table 5.1 Assumed solid mechanics properties pillars and shale rock.

<b>Material type</b>	<b>Young's Modulus (psi)</b>	<b>Poisson's Ratio</b>	<b>Density (g/cc)</b>
<b>Rock Plate</b>	3.00E+06	0.2	2.65
<b>Sand</b>	2.00E+06	0.25	2.65
<b>Ceramic</b>	3.50E+06	0.15	2.65

The flow field has inlet 1 m/s fluid flow through the fracture. The outlet pressure is set to be equal to zero pascal. Fluid viscosity is equal to 1 cP and density is equal to 1 g/cc. The simulated result will provide three sections: stress condition of “Solid Mechanics” part, the velocity field and pressure field of “Laminar Flow” part. See Figure 5.3. It should be mentioned that in real world, the flow condition in fractures is rarely laminar. In the “Laminar Flow” physics the Reynold’s number could be set as a really large value to account for big “Wall effect” in proppant pack. The simulated inlet pressure is the main focus here. As outlet pressure is set to be equal to zero, the average inlet pressure is the pressure difference between two ends. The simulated results are in Table 5.2.

Table 5.2 Pressure difference between two ends for different placement pattern and pillar solid mechanics.

<b>Proppant type and placement pattern</b>	<b>Delta P between inlet and outlet (Pa)</b>			
	<b>500 psi Conf.</b>	<b>1000 psi Conf.</b>	<b>1500psi Conf.</b>	<b>2000psi Conf.</b>
<b>Ceramic random placement</b>	42.7	44.5	46.5	48.8
<b>Ceramic ordered placement</b>	40.9	42.5	44.4	46.7
<b>Sand random placement</b>	42.8	44.7	47	49.5
<b>Sand ordered placement</b>	41	42.7	44.8	47.4

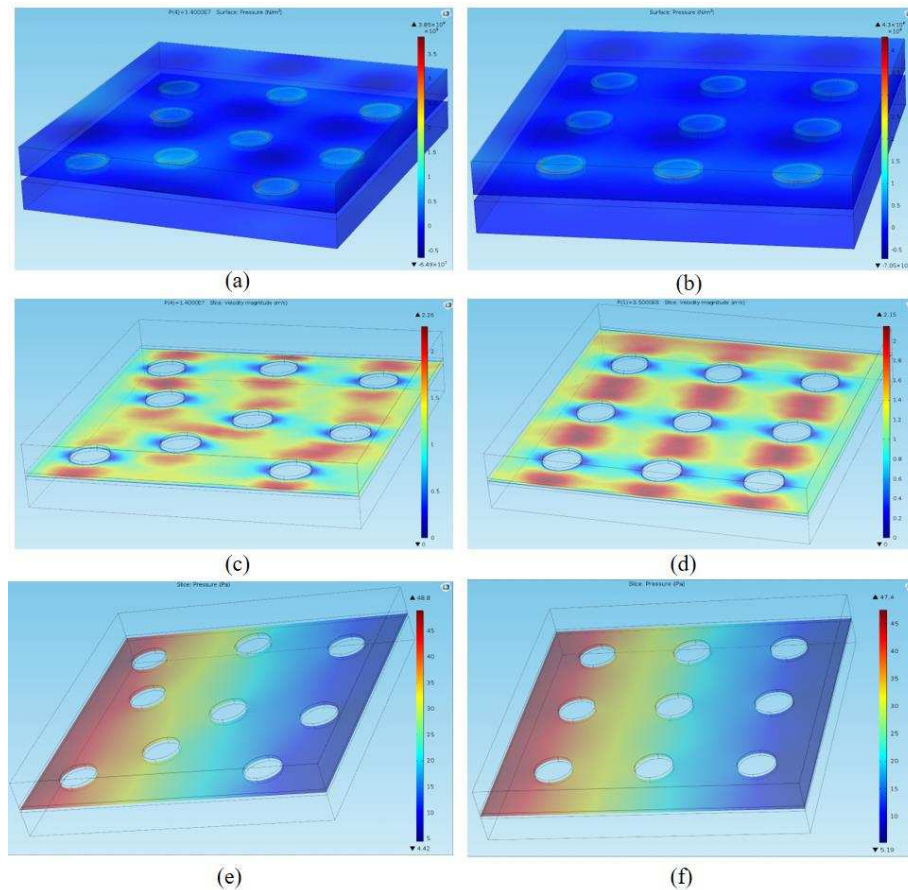


Figure 5.3 Simulation results for disordered pillar placement and random pillar placement at 2000 psi confining: (a) stress condition of random pillar placement; (b) stress condition of ordered pillar placement condition; (c) velocity field of random pillar placement; (d) velocity field of ordered pillar placement; (e) pressure field of random pillar placement; (f) pressure field of ordered pillar placement field.

If one over pressure difference is considered as the normalized permeability, because all other parameters in permeability equation here are controlled to stay the same, the permeability versus confining pressure plot is in Figure 5.4.

The plot shows that when proppant is placed randomly, the average permeability is lower, and when proppant is placed orderly in an array, the average permeability is higher. For each placement pattern, different mechanisms of solid mechanics make differences when confining stress increases. Lower Young's modulus makes the fracture close more quickly; thus, it has more stress sensitivity.

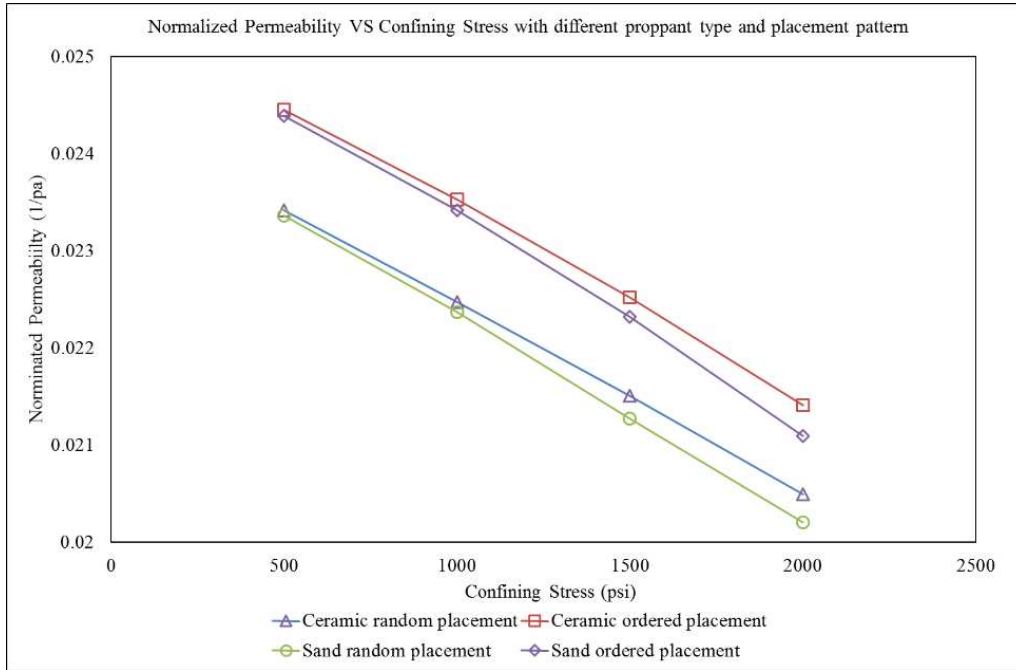


Figure 5.4 Normalized permeability versus confining stress with different proppant types and placement patterns.

Although the placement pattern of clustered proppant fracturing is still not well documented and surely different companies will have different fluid products and pumping strategies that make placement patterns different, the geometry of this model can always be changed to account for that. Same as solid mechanics, not much has been discussed about what should be the Young’s modulus and Poisson’s ratio of a clustered pillar, but as the model is sensitive to these factors, they can always be accounted for.

### 5.3 Discussion

Pillar fracturing is a candidate to sufficiently open our fracture potential; this led us to study this topic. However, as many aspects regarding clustered proppant fracturing are still not yet certain, it is for now meaningful to build a model that could account for the possible dominant parameters of this technique. What’s more, numerical modeling and lab experiments could quote between each other to accelerate our understanding of this technique.

The model built in this research is sensitive to:

- Confining stress
- Flow condition
- Clustered proppant shape
- Clustered proppant placement pattern
- Clustered proppant solid mechanics

## CHAPTER 6

### CONCLUSIONS AND FUTURE WORK

More than thirty sets of experiments were done for different fractures including unpropped ones with different surface topology and propped ones with different proppant types, proppant concentrations and proppant placement patterns. Three topics regarding proppants that could increase the potential SRV system in shale plays have been discussed: 1) conventional proppants with very low concentration; 2) ULW proppant with concentration lower than monolayer; 3) clustered proppant pack.

#### 6.1 Conclusions

The following conclusions have been drawn from this research:

- This work provides unique results on testing the benefits of very low proppant concentration in SRV of unconventional reservoirs.
- ULW 30/80 clearly shows an optimal concentration around 0.01 lb/ft<sup>2</sup> at a given confining stress.
- The fracture roughness effect to the decline pattern of ULW 30/80 was observed and could happen to other types of proppant.
- Clustered proppant design has great potential benefits and should be optimized:
  - 1) its potential to open fractures and create high conductivity channels was observed;
  - 2) a numerical model was built that is sensitive to various possible controlling factors.

#### 6.2 Future Work

From the observations of the lab test and numerical modeling, the following future work is thought to be important:

- Conduct a hybrid proppant transportation test with both conventional proppant and ULW proppant. This test can be combined with the permeability test results in this research to help improve understanding of ULW proppant.
- Categorize clustered proppant placement patterns. Lab proppant transportation tests can use different combinations of proppant and fluid to visualize possible placement patterns. This part relates to solid-fluid coupling physics that is difficult to be numerically modeled. The result could combine with the numerical model built in this research to improve understanding of clustered proppant fracturing techniques.

## REFERENCE

- API. 2015. Hydraulic Fracturing Primer: Unlocking America's Natural Gas Resources (8 Oct 2013 revision), <http://www.api.org/Oil-and-Natural-Gas-Overview/Exploration-and-Production/Hydraulic-Fracturing/Hydraulic-Fracturing-Primer> (Accessed 26 June 2015).
- Barree, R. D., Cox, S. A., Barree, V. L., and Conway, M. W. 2003. Realistic Assessment of Proppant Pack Conductivity for Material Selection. Presented at the SPE Annual Technical Conference and Exhibition, 5-8 October, Denver. SPE-84306-MS. <http://dx.doi.org/10.2118/84306-MS>.
- Biot, M. A. 1941. General Theory of Three-Dimensional Consolidation. *Journal of Applied Physics*. **12** (2): 155-164. <http://dx.doi.org/10.1063/1.1712886>.
- Brannon, H. D., Malone, M. R., Rickards, A. R. et al. 2004. Maximizing Fracture Conductivity with Proppant Partial Monolayers: Theoretical Curiosity or Highly Productive Reality? Presented at the SPE Annual Technical Conference and Exhibition, 26-29 September, Houston, Texas. SPE-90698-MS. <http://dx.doi.org/10.2118/90698-MS>.
- Brannon, H. D., Kendrick, D. E., Luckey, E., and Stipetich, A. 2009. Multistage Fracturing of Horizontal Shale Gas Wells Using >90% Foam Provides Improved Production. Presented at the SPE Eastern Regional Meeting, 23-25 September, Charleston, West Virginia. SPE-124767-MS. <http://dx.doi.org/10.2118/124767-MS>.
- Cho, Y., Ozkan, E., and Apaydin, O. G. 2013. Pressure-Dependent Natural-Fracture Permeability in Shale and Its Effect on Shale-Gas Well Production. *SPE Reservoir Evaluation & Engineering*. **16** (02): 216-228. SPE-159801-PA. <http://dx.doi.org/10.2118/159801-PA>.
- Chapuis, R. P., and Aubertin, M. 2003. "On the Use of the Kozeny-Carman Equation to Predict the Hydraulic Conductivity of Soils," *Canadian Geotechnical Journal*. **40** (3): 616-628. <http://dx.doi.org/10.1139/t03-013>.
- Cipolla, C., and Wallace, J. 2014. Stimulated Reservoir Volume: A Misapplied Concept? Presented at the SPE Hydraulic Fracturing Technology Conference, 4-6 February, The Woodlands, Texas. SPE-168596-MS. <http://dx.doi.org/10.2118/168596-MS>.
- Coulter, G. R., Gross, B. C., Benton, E. G., and Thomson, C. L. 2004. Water Fracs and Sand Quantity: A Barnett Shale Example. Presented at the SPE Annual Technical Conference and Exhibition, 26-29 September, Houston. SPE-90891-MS. <http://dx.doi.org/10.2118/90891-MS>.
- Corapcioglu, H., Miskimins, J., and Prasad, M. 2014. Fracturing Fluid Effects on Young's

Modulus and Embedment in the Niobrara Formation. Presented at the SPE Annual Technical Conference and Exhibition, 27-29 October, Amsterdam, The Netherlands. SPE-170835-MS. <http://dx.doi.org/10.2118/170835-MS>.

Cui, Q. 2015. Smart depletion study of shale well. In progress.

Davies, J. P., and Davies, D. K. 2001. Stress-Dependent Permeability: Characterization and Modeling. SPE Journal. 6 (02): 224-235. SPE-71750-PA. <http://dx.doi.org/10.2118/71750-PA>.

Duenckel, R., Conway, M. W., Eldred, B., and Vincent, M. C. 2012. Proppant Diagenesis--Integrated Analyses Provide New Insights Into Origin, Occurrence, and Implications for Proppant Performance. SPE Production & Operations. 27 (02): 131-144. SPE-139875-PA. <http://dx.doi.org/10.2118/139875-PA>.

Darin, S. R., and Huitt, J. L. 1960. Effect of a Partial Monolayer of Propping Agent on Fracture Flow Capacity. Petroleum Transactions, AIME. 219: 31-37. SPE 1291-G.

EEC Environmental. 2010. A Brief History of Hydraulic Fracturing (22 Nov, 2011 revision), <http://www.eecworld.com/services/258-a-brief-history-of-hydraulic-fracturing> (Accessed 13 June 2015).

EIA. U.S. Energy Information Administration. 2014. New Eagle Ford wells continue to show higher production (29 Sep, 2014 revision), <https://www.eia.gov/todayinenergy/detail.cfm?id=18171> (Accessed 18 June 2015).

Economides, M. J., 2007. Modern fracturing: Enhancing natural gas production (pp. 289). Houston, Texas: ET Publishing.

Gaurav, A., Dao, E. K., and Mohanty, K. K. 2010. Ultra-Lightweight Proppants for Shale Gas Fracturing. Presented at the Tight Gas Completions Conference, 2-3 November, San Antonio, Texas. SPE-138319-MS, <http://dx.doi.org/10.2118/138319-MS>.

Howard, G.C., Fast, C.R.: "Hydraulic Fracturing", SPE Monograph, Volume 2, 1970.

Huang, J., Deshpande, K. M., Safari, R. et al. 2015. Clustered Proppant Design Optimization Utilizing Advanced Geomechanics-Flow-Reservoir Modeling. Presented at the SPE Liquids-Rich Basins Conference--North America, 2-3 September, Midland, Texas. SPE-175528-MS. <http://dx.doi.org/10.2118/175528-MS>.

Inyang, U. A., Nguyen, P. D., and Cortez, J. 2014. Development and Field Applications of Highly Conductive Proppant-free Channel Fracturing Method. Presented at the SPE Unconventional Resources Conference, 1-3 April, The Woodlands, Texas. SPE-168996-MS. <http://dx.doi.org/10.2118/168996-MS>.

- ISO 2015. ISO 13503-5:2006 Petroleum and natural gas industries -- Completion fluids and materials -- Part 5: Procedures for measuring the long-term conductivity of proppants (1 Jul. 2006 Revision).  
[http://www.iso.org/iso/iso\\_catalogue/catalogue\\_tc/catalogue\\_detail.htm?csnumber=40531](http://www.iso.org/iso/iso_catalogue/catalogue_tc/catalogue_detail.htm?csnumber=40531) (Assessed 4 Jul. 2015).
- Jansen, T. A., Zhu, D., and Hill, A. D. 2015. The Effect of Rock Mechanical Properties on Fracture Conductivity for Shale Formations. Presented at the SPE Hydraulic Fracturing Technology Conference, 3-5 February, The Woodlands, Texas. SPE-173347-MS. <http://dx.doi.org/10.2118/173347-MS>.
- Kamenov, A., Zhu, D., Hill, A. D., and Zhang, J. 2013. Laboratory Measurement of Hydraulic Fracture Conductivities in the Barnett Shale. Presented at the SPE Hydraulic Fracturing Technology Conference, 4-6 February, The Woodlands, Texas. SPE-163839-MS. <http://dx.doi.org/10.2118/163839-MS>.
- Mayerhofer, M. J., Lolon, E., Warpinski, N. R., Cipolla, C. L. et al. What Is Stimulated Reservoir Volume? *SPE Production & Operations*. **25** (01): 89-98. SPE-119890-PA. <http://dx.doi.org/10.2118/119890-PA>.
- Medvedev, A. V., Kraemer, C. C., Pena, A. A., and Panga, M. K. R. 2013. On the Mechanisms of Channel Fracturing. Presented at the SPE Hydraulic Fracturing Technology Conference, 4-6 February, The Woodlands, Texas. SPE-163836-MS. <http://dx.doi.org/10.2118/163836-MS>.
- Palisch, T. T., Vincent, M., and Handren, P. J. 2010. Slickwater Fracturing: Food for Thought. Society of Petroleum Engineers. *SPE Production & Operations*. **25** (03): 327-344. SPE-115766-PA. <http://dx.doi.org/10.2118/115766-PA>.
- Pyrak-Nolte, L. J., Morris, J. P. 2000. Single fractures under normal stress: The relation between fracture specific stiffness and fluid flow. *International Journal of Rock Mechanics and Mining Sciences*. **37** (1), 245-262. [http://dx.doi.org/10.1016/S1365-1609\(99\)00104-5](http://dx.doi.org/10.1016/S1365-1609(99)00104-5).
- Sarkar, S., Toksöz, M. N., and Burns, D. R. 2004. Fluid Flow Modeling in Fractures. Earth Resources Laboratory Dept. of Earth, Atmospheric and Planetary Sciences. Massachusetts Institute of Technology. Cambridge, MA 02139.
- Schlumberger. 2015. HiWAY Flow-Channel Fracturing Technique (15 Oct. 2015 revision). [http://www.slb.com/services/completions/stimulation/sandstone/hiway\\_channel\\_fracturing.aspx?t=2](http://www.slb.com/services/completions/stimulation/sandstone/hiway_channel_fracturing.aspx?t=2) (Assessed 12 Sep. 2015).
- Tian, Y. 2014. Experimental Study on Stress Sensitivity of Naturally Fractured Reservoirs. SPE

Annual Technical Conference and Exhibition, 27-29 Oct, Amsterdam, The Netherlands. SPE-173463-STU. <http://dx.doi.org/10.2118/173463-STU>.

Terzaghi, C. 1925. Principles of soil mechanics. *Engineering News-Record*, Vol. 95, Nos. 19-23, 25-27, pp. 742-746, 796-800, 832-836, 874-878, 912-915, 987-990, 1026-1029, 1064-1068. Also published in book form : New York, McGraw-Hill, 1926. 98 pp.

Trujillo, H., Tengono, J. A., Rubiano, J. et al. 2011. How to Deliver 100% Packing Efficiency in Openhole Gravel Packs: A Field Study in Colombia. Presented at the SPE Annual Technical Conference and Exhibition, 30 October-2 November, Denver, Colorado. SPE-146447-MS. <http://dx.doi.org/10.2118/146447-MS>.

Vincent, M. C., and Besler, M. R. 2013. Declining Frac Effectiveness - Evidence that Propped Fractures Lose Conductivity, Surface Area, and Hydraulic Continuity. Presented at the Unconventional Resources Technology Conference, 12-14 August, Denver, Colorado. SPE-168744-MS. <http://dx.doi.org/10.1190/URTEC2013-073>.

YouTube. 2015. Fracking with Less Water (7 Jun 2012 revision). [https://www.youtube.com/watch?v=ADGfbj5c\\_R4](https://www.youtube.com/watch?v=ADGfbj5c_R4) (Assessed 8 Oct. 2015).

Zhang, J. 2014. Fracture Conductivity Damage by Water in Shale Formations. Presented at the SPE Annual Technical Conference and Exhibition, 27-29 October, Amsterdam, The Netherlands. SPE-173473-STU. <http://dx.doi.org/10.2118/173473-STU>.

## APPENDIX A

### DERIVATION OF CRITICAL MONOLAYER PROPPANT CONCENTRATION

Two patterns are considered here: 1) loose placement; 2) tight placement. See Figure A.1.

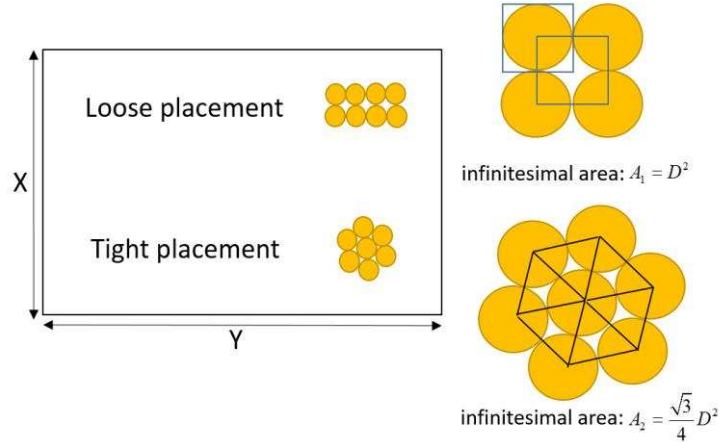


Figure A.1 Schematic of infinitesimal area calculation for loose and tight monolayer placement.

If the fracture width is assumed to be the medium proppant diameter, the fracture surface area is assumed to be infinitely larger than proppant diameter, and the fracture surface is assumed to be fully packed. The critical point for this derivation lies on the determination of proppant numbers on the fracture.

For loose placement, the total proppant number equals:

$$n_1 = \frac{XY}{A_1} = \frac{XY}{D^2} \quad (\text{A.1})$$

Proppant concentration equals:

$$C_1 = \frac{n_1 V_p \rho}{XY} = \frac{\frac{XY}{D^2} \left( \frac{4}{3} \pi \left( \frac{D}{2} \right)^3 \right) \rho}{XY} = \frac{\pi}{6} D \rho \quad (\text{A.2})$$

When  $D$  is in cm and  $\rho$  is in g/cc, considering conversion from g/cm<sup>2</sup> to lb/ft<sup>2</sup>, this equation becomes

$$C_1 = 1.0724 D \rho \quad (\text{A.3})$$

For tight placement, the total proppant number equals:

$$n_2 = \frac{XY}{A_2} = \frac{XY}{\frac{\sqrt{3}}{4} D^2} \quad (\text{A.4})$$

Proppant concentration equals:

$$C_2 = \frac{n_2 V_p \rho}{XY} = \frac{\frac{XY}{\frac{\sqrt{3}}{4} D^2} \left( \frac{4}{3} \pi \left( \frac{D}{2} \right)^3 \right) \rho}{XY} = \frac{2\sqrt{3}}{9} \pi D \rho \quad (\text{A.5})$$

Considering unit conversion, the equation becomes:

$$C_2 = 2.4766 D \rho \quad (\text{A.6})$$

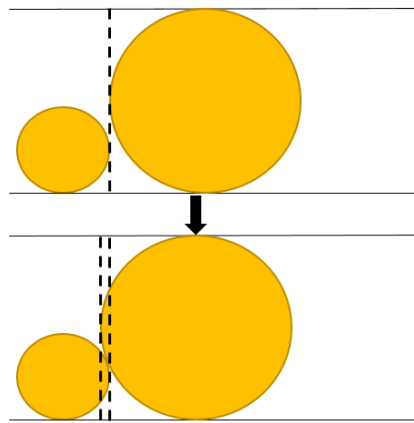


Figure A.2 Schematic of how size range effect concentration calculation.

However, in the real world, each proppant product has a size range due to a certain manufacture process. This could potentially make the real concentration for monolayer higher. See Figure A.2. However, this could relatively be ignored if the proppant size is more grouped to the medium diameter.

To obtain a small amount of representative proppant samples, a proppant sorting device was used. See Figure A.3. Every proppant product has a special mesh size distribution within its mesh size range. This device is used to obtain a small amount of proppant that has the most representative mesh size distribution of the product. The proppants being sorted were kept

poured into the top of the device and were separated into two groups, then one group was sorted by the device again. This process kept going until a small amount of representative proppant samples were obtained.



Figure A.3 Proppant sample sorting device.

To form a full monolayer proppant pack, the concentration should be between  $C_1$  and  $C_2$ , namely:

$$1.0724D\rho \leq C \leq 2.4766D\rho \quad (\text{A.7})$$

Where  $D$  is proppant medium diameter in inches,  $\rho$  is proppant density in  $\text{g/cm}^3$ .  $C$  is critical monolayer concentration in  $\text{lb/ft}^2$ . This equation eliminates the porosity estimation by Brannon et al. (2004).